

A NEW NUMERICAL METHOD FOR DIV-CURL SYSTEMS WITH LOW REGULARITY ASSUMPTIONS

SHUHAO CAO, CHUNMEI WANG, AND JUNPING WANG

ABSTRACT. This paper presents a numerical method for div-curl systems with normal boundary conditions by using a finite element technique known as primal-dual weak Galerkin (PDWG). The PDWG finite element scheme for the div-curl system has two prominent features in that it offers not only an accurate and reliable numerical solution to the div-curl system under the low H^α -regularity ($\alpha > 0$) assumption for the true solution, but also an effective approximation of normal harmonic vector fields regardless the topology of the domain. Results of seven numerical experiments are presented to demonstrate the performance of the PDWG algorithm, including one example on the computation of discrete normal harmonic vector fields.

1. INTRODUCTION

In this paper we are concerned with the development of new numerical methods for div-curl systems equipped with normal boundary conditions. For simplicity, consider the model problem that seeks a vector field $\mathbf{u} = \mathbf{u}(\mathbf{x})$ satisfying

$$(1.1) \quad \nabla \cdot (\varepsilon \mathbf{u}) = f, \quad \text{in } \Omega,$$

$$(1.2) \quad \nabla \times \mathbf{u} = \mathbf{g}, \quad \text{in } \Omega,$$

$$(1.3) \quad \varepsilon \mathbf{u} \cdot \mathbf{n} = \phi_1, \quad \text{on } \Gamma,$$

where $\Omega \subset \mathbb{R}^3$ is a polyhedral domain that is bounded, open, and connected. $\Gamma = \partial\Omega$ is the boundary of Ω and is assumed to be the union of a finite number of disjoint surfaces $\Gamma = \bigcup_{i=0}^L \Gamma_i$, where Γ_0 is the exterior boundary of Ω , Γ_i ($i = 1, \dots, L$) are the other connected components with finite surface areas, and L denotes the number of holes in the domain Ω geometrically and is known as the second Betti number of Ω or the dimension of the second de Rham cohomology group of Ω . The Lebesgue-integrable real-valued function $f = f(\mathbf{x})$ and the vector field $\mathbf{g} = \mathbf{g}(\mathbf{x})$ are given in the domain Ω , the coefficient matrix $\varepsilon = \{\varepsilon_{ij}(\mathbf{x})\}_{3 \times 3}$ is symmetric and uniformly positive definite in Ω , and the entries $\varepsilon_{ij}(\mathbf{x})$ ($i, j = 1, \dots, 3$) are in $L^\infty(\Omega)$. The normal boundary data ϕ_1 is a given distribution in $H^{-\frac{1}{2}}(\Gamma)$.

2020 *Mathematics Subject Classification.* Primary 65N30, 35Q60, 65N12; Secondary 35F45, 35Q61.

Key words and phrases. finite element methods, weak Galerkin methods, primal-dual weak Galerkin, div-curl system.

The research of Shuhao Cao was partially supported by National Science Foundation Award DMS-1913080.

The research of Chunmei Wang was partially supported by National Science Foundation Award DMS-1849483.

The research of Junping Wang was supported by the NSF IR/D program, while working at National Science Foundation. However, any opinion, finding, and conclusions or recommendations expressed in this material are those of the author and do not necessarily reflect the views of the National Science Foundation.

The solution uniqueness for the normal boundary value problem (1.1)-(1.3) depends on the topology of the domain Ω . It is well-known that the solution uniqueness holds true for simply connected Ω , while the solution is unique up to a normal ε -harmonic function in $\mathbb{H}_{\varepsilon n,0}(\Omega)$ defined in (2.2) when the domain Ω is not simply connected. The dimension of $\mathbb{H}_{\varepsilon n,0}(\Omega)$ is identical to the first Betti number of Ω , which is the rank of the first homology group of Ω or the dimension of the first de Rham cohomology group of Ω .

The div-curl system (1.1)-(1.2) arises in many applications such as electromagnetic fields and fluid mechanics. Computational electro-magnetics plays an important role in many areas of science and engineering such as radar, satellite, antenna design, waveguides, optical fibers, medical imaging and design of invisible cloaking devices [14]. In linear magnetic fields, the function $f(\mathbf{x})$ vanishes, \mathbf{u} represents the magnetic field intensity and $\varepsilon(\mathbf{x})$ is the inverse of the magnetic permeability tensor. In fluid mechanics fields, the coefficient matrix $\varepsilon(\mathbf{x})$ is diagonal with diagonal entries being the local mass density. In electrostatics fields, $\varepsilon(\mathbf{x})$ is the permittivity matrix.

Several numerical methods based on finite element approaches have been proposed and analyzed for the div-curl system (1.1)-(1.2). For example, a covolume method was developed in three dimensional space by using the Voronoi-Delaunay mesh pairs [18]. In [5], a finite element method based on different test and trial spaces was analyzed for a div-curl system. In [16], the authors introduced a mimetic finite difference scheme for the three dimensional magneto-static problems on general polyhedral partitions. In [10], the authors developed a mixed finite element method for three dimensional axisymmetric div-curl systems through a dimension reduction technique based on the cylindrical coordinates in simply connected and axisymmetric domains. In [4], the authors developed a least-squares finite element method for two types boundary value problems. Another least-squares method was proposed for the div-curl problem based on discontinuous elements on nonconvex polyhedral domains in [3]. In [21], the authors proposed a weak Galerkin finite element method for the div-curl system with either normal or tangential boundary conditions. Another weak Galerkin scheme was introduced in [15] by using a least-squares approach for the div-curl problem. In [17], the authors developed a primal-dual weak Galerkin finite element method for the div-curl system with tangential boundary conditions and proved that the scheme works well with low-regularity assumptions on the exact solution.

Two major challenges for the div-curl model problem (1.1)-(1.3) are the low-regularity of the true solution \mathbf{u} and the difficulties in approximating the normal ε -harmonic vector space $\mathbb{H}_{\varepsilon n,0}(\Omega)$ due to the topological complexity of the domain Ω . The goal of this paper is to address both challenges through a new numerical method based on the primal-dual weak Galerkin (PDWG) finite element approach originated in [23] and further developed in [20, 25, 26, 7, 22, 13] for various model problems. Our PDWG numerical method for (1.1)-(1.3) has two prominent features over the existing numerical methods: (1) it offers an effective approximation of the normal ε -harmonic vector space $\mathbb{H}_{\varepsilon n,0}(\Omega)$ regardless of the topology of the domain Ω ; and (2) it provides an accurate and reliable numerical solution for the div-curl system (1.1)-(1.3) with low H^α -regularity ($\alpha > 0$) assumption for the true solution \mathbf{u} .

The paper is organized as follows. Section 2 is devoted to notations and the derivation of a weak formulation for the div-curl system (1.1)-(1.3) that involves no partial derivatives over the vector field \mathbf{u} . Section 3 offers a brief review on the discrete weak gradient and discrete weak curl operators. Section 4 is dedicated to the presentation of the PDWG algorithm for the div-curl problem, together with an algorithm for computing discrete normal ε -harmonic

vector fields. Section 5 is devoted to a discussion of the solution existence and uniqueness for the PDWG scheme. Section 6 contains a convergence theory for the PDWG approximation, and Section 7 demonstrates the performance of the PDWG algorithm through seven test examples.

2. NOTATIONS AND PRELIMINARIES

We follow the usual notation for Sobolev spaces and norms, see for example [9, 12]. For an open bounded domain $D \subset \mathbb{R}^3$ with Lipschitz continuous boundary and any given real number $s \geq 0$, we use $\|\cdot\|_{s,D}$ and $|\cdot|_{s,D}$ to denote the norm and seminorm in the Sobolev space $H^s(D)$, respectively. The space $H^0(D)$ coincides with $L^2(D)$, for which the norm and the inner product are denoted by $\|\cdot\|_D$ and $(\cdot, \cdot)_D$, respectively. We use $H(\operatorname{div}_\varepsilon; D)$ to denote the closed subspace of $[L^2(D)]^2$ so that $\nabla \cdot (\varepsilon \mathbf{v}) \in L^2(D)$. The space $H(\operatorname{div}; D)$ corresponds to the case of $\varepsilon = I$. Analogously, we use $H(\operatorname{curl}; D)$ to denote the closed subspace of $[L^2(D)]^2$ so that $\nabla \times \mathbf{v} \in [L^2(D)]^3$. Denote by

$$H_0(\operatorname{curl}; D) := \{\mathbf{v} \in H(\operatorname{curl}; D), \mathbf{v} \times \mathbf{n} = 0 \text{ on } \partial D\}$$

the closed subspace with vanishing tangential boundary values. When $D = \Omega$, we shall drop the script D in the notations. For simplicity, we shall use “ \lesssim ” to denote “less than or equal to up to a general constant independent of the mesh size or functions appearing in the inequality”.

Introduce the following Sobolev space

$$(2.1) \quad \mathbb{W}_\varepsilon(\Omega) = \{\mathbf{v} \in H_0(\operatorname{curl}) \cap H(\operatorname{div}_\varepsilon), \nabla \cdot (\varepsilon \mathbf{v}) = 0, \langle \varepsilon \mathbf{v} \cdot \mathbf{n}_i, 1 \rangle_{\Gamma_i} = 0, i = 1, \dots, L\}.$$

A vector field $\mathbf{v} \in [L^2(\Omega)]^3$ is said to be ε -harmonic on Ω if it is ε -solenoidal and irrotational on Ω . The space of normal ε -harmonic vector fields, denoted by $\mathbb{H}_{\varepsilon n, 0}(\Omega)$, consists of all ε -harmonic vector fields satisfying the zero normal boundary condition; i.e.,

$$(2.2) \quad \mathbb{H}_{\varepsilon n, 0}(\Omega) = \{\mathbf{v} \in [L^2(\Omega)]^3 : \nabla \times \mathbf{v} = 0, \nabla \cdot (\varepsilon \mathbf{v}) = 0, \varepsilon \mathbf{v} \cdot \mathbf{n} = 0 \text{ on } \Gamma\}.$$

When $\varepsilon = I$ is the identity matrix, the space $\mathbb{H}_{\varepsilon n, 0}(\Omega)$ shall be denoted as $\mathbb{H}_{n, 0}(\Omega)$. Analogously, the space of tangential ε -harmonic vector fields, denoted by $\mathbb{H}_{\varepsilon \tau, 0}(\Omega)$, consists of all ε -harmonic vector fields satisfying the zero tangential boundary condition; i.e.,

$$\mathbb{H}_{\varepsilon \tau, 0}(\Omega) = \{\mathbf{v} \in [L^2(\Omega)]^3 : \nabla \times \mathbf{v} = 0, \nabla \cdot (\varepsilon \mathbf{v}) = 0, \mathbf{v} \times \mathbf{n} = 0 \text{ on } \Gamma\}.$$

2.1. A weak formulation. By testing the equation (1.1) against any $\varphi \in H^1(\Omega)$ and then using the normal boundary condition (1.3) we obtain

$$(2.3) \quad (\mathbf{u}, \varepsilon \nabla \varphi) = \langle \phi_1, \varphi \rangle - (f, \varphi), \quad \forall \varphi \in H^1(\Omega).$$

Next, we test the equation (1.2) against any $\mathbf{w} \in H_0(\operatorname{curl}; \Omega)$ to obtain

$$(2.4) \quad (\mathbf{u}, \nabla \times \mathbf{w}) = (\mathbf{g}, \mathbf{w}), \quad \forall \mathbf{w} \in H_0(\operatorname{curl}; \Omega).$$

Summing the equations (2.3) and (2.4) gives the following

$$(\mathbf{u}, \varepsilon \nabla \varphi + \nabla \times \mathbf{w}) = (\mathbf{g}, \mathbf{w}) - (f, \varphi) + \langle \phi_1, \varphi \rangle$$

for all $\varphi \in H^1(\Omega)$ and $\mathbf{w} \in H_0(\operatorname{curl}; \Omega)$.

Definition 2.1. A vector-valued function $\mathbf{u} \in [L^2(\Omega)]^3$ is said to be a weak solution of the normal boundary value problem for the div-curl system (1.1)-(1.3) if it satisfies the following equation

$$(2.5) \quad (\mathbf{u}, \varepsilon \nabla \varphi + \nabla \times \boldsymbol{\psi}) = (\mathbf{g}, \boldsymbol{\psi}) - (f, \varphi) + \langle \phi_1, \varphi \rangle$$

for all $\varphi \in H^1(\Omega)$ and $\boldsymbol{\psi} \in H_0(\text{curl}; \Omega)$.

The solution to the variational problem (2.5) is generally non-unique. In fact, the homogeneous version of (2.5) seeks $\mathbf{u} \in [L^2(\Omega)]^3$ satisfying

$$(2.6) \quad (\mathbf{u}, \varepsilon \nabla \varphi + \nabla \times \boldsymbol{\psi}) = 0 \quad \forall \varphi \in H^1(\Omega), \boldsymbol{\psi} \in H_0(\text{curl}; \Omega).$$

The equation (2.6) is easily satisfied by any ε -harmonic function $\mathbf{u} = \boldsymbol{\eta} \in \mathbb{H}_{\varepsilon n, 0}(\Omega)$, and hence the solution non-uniqueness when the ε -harmonic space $\mathbb{H}_{\varepsilon n, 0}(\Omega)$ has a positive dimension. The solution to the div-curl system with normal boundary condition is unique when the solution is further required to be ε -weighted L^2 orthogonal to $\mathbb{H}_{\varepsilon n, 0}(\Omega)$.

2.2. An extended weak formulation. Denote by $H_{0c}^1(\Omega)$ the space of functions in $H^1(\Omega)$ with vanishing value on Γ_0 and constant values on other connected components of the boundary; i.e.,

$$H_{0c}^1(\Omega) = \{\phi \in H^1(\Omega) : \phi|_{\Gamma_0} = 0, \phi|_{\Gamma_i} = \alpha_i, i = 1, \dots, L\}.$$

Introduce the following bilinear form:

$$(2.7) \quad B(\mathbf{u}, s; \varphi, \boldsymbol{\psi}) := (\mathbf{u}, \varepsilon \nabla \varphi + \nabla \times \boldsymbol{\psi}) + (\boldsymbol{\psi}, \varepsilon \nabla s).$$

The extended weak formulation for the normal boundary value problem of the div-curl system seeks $(\mathbf{u}, s) \in [L^2(\Omega)]^3 \times H_{0c}^1(\Omega)$ such that

$$(2.8) \quad B(\mathbf{u}, s; \varphi, \boldsymbol{\psi}) = F(\varphi, \boldsymbol{\psi}) \quad \forall \varphi \in H^1(\Omega), \forall \boldsymbol{\psi} \in H_0(\text{curl}; \Omega),$$

where

$$F(\varphi, \boldsymbol{\psi}) = (\mathbf{g}, \boldsymbol{\psi}) - (f, \varphi) + \langle \phi_1, \varphi \rangle.$$

Note that by testing the curl equation in the div-curl system against any $\rho \in H_{0c}^1(\Omega)$ we have

$$(2.9) \quad (\mathbf{g}, \nabla \rho) = 0, \quad \forall \rho \in H_{0c}^1(\Omega),$$

which gives rise to the following compatibility condition:

$$(2.10) \quad \nabla \cdot \mathbf{g} = 0, \quad \langle \mathbf{g} \cdot \mathbf{n}_i, 1 \rangle_{\Gamma_i} = 0, \text{ for } i = 1, \dots, L.$$

Theorem 2.1. *Under the compatibility condition (2.10) for \mathbf{g} , the solution $(\mathbf{u}; s)$ of (2.8) satisfies the following equations:*

$$(2.11) \quad \nabla \cdot (\varepsilon \mathbf{u}) = f, \quad \text{in } \Omega,$$

$$(2.12) \quad \nabla \times \mathbf{u} = \mathbf{g}, \quad \text{in } \Omega,$$

$$(2.13) \quad s = 0, \quad \text{in } \Omega,$$

$$(2.14) \quad \varepsilon \mathbf{u} \cdot \mathbf{n} = \phi_1, \quad \text{on } \Gamma.$$

Proof. By letting $\boldsymbol{\psi} = 0$ in (2.8) we have

$$(\mathbf{u}, \varepsilon \nabla \varphi) = -(f, \varphi) + \langle \phi_1, \varphi \rangle_{\Gamma}$$

for all $\varphi \in H^1(\Omega)$. It follows that $\nabla \cdot (\varepsilon \mathbf{u}) = f$ and $\varepsilon \mathbf{u} \cdot \mathbf{n} = \phi_1$ on Γ , which leads to (2.11) and (2.14). Next, by letting $\varphi = 0$ in (2.8) we arrive at

$$(\mathbf{u}, \nabla \times \boldsymbol{\psi}) + (\boldsymbol{\psi}, \varepsilon \nabla s) = (\mathbf{g}, \boldsymbol{\psi}), \quad \forall \boldsymbol{\psi} \in H_0(\text{curl}; \Omega),$$

which leads to

$$(\nabla \times \mathbf{u} + \varepsilon \nabla s, \boldsymbol{\psi}) = (\mathbf{g}, \boldsymbol{\psi}),$$

and thus

$$(2.15) \quad \nabla \times \mathbf{u} + \varepsilon \nabla s = \mathbf{g}, \quad \text{in } \Omega.$$

Now from (2.15) we have

$$(\nabla \times \mathbf{u} + \varepsilon \nabla s, \nabla s) = (\mathbf{g}, \nabla s),$$

which, by the usual integration by parts, gives

$$\langle \mathbf{n} \times \mathbf{u}, \nabla s \rangle_{\Gamma} + (\varepsilon \nabla s, \nabla s) = (\mathbf{g}, \nabla s),$$

and by the boundary condition of $s = \text{const}$ on each Γ_i and the compatibility condition (2.10)

$$(\varepsilon \nabla s, \nabla s) = \langle \mathbf{u}, \mathbf{n} \times \nabla s \rangle_{\Gamma} + (\mathbf{g}, \nabla s) = 0.$$

It follows that $\nabla s = 0$ so that $s \equiv 0$. This completes the proof of the theorem. \square

The homogeneous dual problem of (2.8) seeks $\lambda \in H^1(\Omega)/\mathbb{R}$ and $\mathbf{q} \in H_0(\text{curl}; \Omega)$ satisfying

$$(2.16) \quad B(\mathbf{v}, r; \lambda, \mathbf{q}) = 0 \quad \forall \mathbf{v} \in [L^2(\Omega)]^3, r \in H_{0c}^1(\Omega).$$

Theorem 2.2. *The solution to the homogeneous dual problem (2.16) is unique.*

Proof. The problem (2.16) can be rewritten as

$$(2.17) \quad (\mathbf{v}, \varepsilon \nabla \lambda + \nabla \times \mathbf{q}) + (\mathbf{q}, \varepsilon \nabla r) = 0$$

for all $\mathbf{v} \in [L^2(\Omega)]^3$ and $r \in H_{0c}^1(\Omega)$. Note that the test against $r \in H_{0c}^1(\Omega)$ and $\mathbf{v} = 0$ ensures $\nabla \cdot (\varepsilon \mathbf{q}) = 0$ and $\langle \varepsilon \mathbf{q} \cdot \mathbf{n}, 1 \rangle_{\Gamma_i} = 0$ for all $i \in \{1, \dots, L\}$. In addition, by letting $r = 0$ and varying $\mathbf{v} \in [L^2(\Omega)]^3$ we arrive at

$$\varepsilon \nabla \lambda + \nabla \times \mathbf{q} = 0,$$

which, by testing against $\nabla \lambda$, leads to

$$(\varepsilon \nabla \lambda, \nabla \lambda) = 0,$$

so that $\lambda \equiv 0$ and hence

$$\nabla \times \mathbf{q} = 0.$$

Thus, we have

$$\mathbf{q} \in \mathbb{H}_{\varepsilon\tau, 0}(\Omega), \quad \langle \varepsilon \mathbf{q} \cdot \mathbf{n}_i, 1 \rangle_{\Gamma_i} = 0 \text{ for } i = 1, \dots, L,$$

which yields $\mathbf{q} \equiv 0$. \square

3. DISCRETE WEAK GRADIENT AND WEAK CURL

The extended weak formulation (2.8) is based on the gradient and curl differential operators. In this section, we shall review the notion of discrete weak gradient and weak curl which forms a corner stone of the weak Galerkin finite element method. To this end, let T be a polyhedral domain with boundary ∂T and unit outward normal direction \mathbf{n} on ∂T . Define the space of weak functions in T by

$$W(T) = \{v = \{v_0, v_b\} : v_0 \in L_2(T), v_b \in L_2(\partial T)\},$$

where v_0 represents the value of v in the interior of T , and v_b represents some specific boundary information of v . Analogously, define the space of vector-valued weak functions on T by

$$V(T) = \{\mathbf{v} = \{\mathbf{v}_0, \mathbf{v}_b\} : \mathbf{v}_0 \in [L_2(T)]^3, \mathbf{v}_b \in [L_2(\partial T)]^3\}.$$

Let $P_j(T)$ the space of polynomials on T with total degree j and less. For any $v \in W(T)$, the discrete weak gradient, denoted by $\nabla_{w,j,T}v$, is defined as the unique vector-valued polynomial in $[P_j(T)]^3$ satisfying

$$(3.1) \quad (\nabla_{w,j,T}v, \boldsymbol{\varphi})_T = -(v_0, \nabla \cdot \boldsymbol{\varphi})_T + \langle v_b, \boldsymbol{\varphi} \cdot \mathbf{n} \rangle_{\partial T}, \quad \forall \boldsymbol{\varphi} \in [P_j(T)]^3.$$

Analogously, the discrete weak curl of $\mathbf{v} \in V(T)$, denoted by $\nabla_{w,j,T} \times \mathbf{v}$, is defined as the unique vector-valued polynomial in $[P_j(T)]^3$, satisfying

$$(3.2) \quad (\nabla_{w,j,T} \times \mathbf{v}, \boldsymbol{\varphi})_T = (\mathbf{v}_0, \nabla \times \boldsymbol{\varphi})_T - \langle \mathbf{v}_b \times \mathbf{n}, \boldsymbol{\varphi} \rangle_{\partial T}, \quad \forall \boldsymbol{\varphi} \in [P_j(T)]^3.$$

4. PDWG NUMERICAL ALGORITHM

Let \mathcal{T}_h be a finite element partition of the domain Ω consisting of polyhedra that are shape-regular [27]. Denote by \mathcal{E}_h the set of faces in \mathcal{T}_h and $\mathcal{E}_h^0 = \mathcal{E}_h \setminus \partial\Omega$ the set of interior faces. Denote by h_T the diameter of the element $T \in \mathcal{T}_h$ and $h = \max_{T \in \mathcal{T}_h} h_T$ the meshsize of the partition \mathcal{T}_h .

For a given integer $k \geq 0$, we introduce the following finite element spaces subordinated to \mathcal{T}_h :

$$\mathbf{V}_h = \{\mathbf{v} : \mathbf{v}|_T \in [P_k(T)]^3, \forall T \in \mathcal{T}_h\},$$

$$S_h = \{\{s_0, s_b\} : s_0|_T \in P_k(T), s_b|_{\partial T} \in P_k(\partial T), \forall T \in \mathcal{T}_h, s_b|_{\Gamma_0} = 0, s_b|_{\Gamma_i} = c_i\},$$

$$M_h = \{\{\varphi_0, \varphi_b\} : \varphi_0|_T \in P_k(T), \varphi_b|_{\partial T} \in P_k(\partial T), \forall T \in \mathcal{T}_h, \int_{\Omega} \varphi_0 = 0\},$$

$$\mathbf{W}_h = \{\boldsymbol{\psi} = \{\boldsymbol{\psi}_0, \boldsymbol{\psi}_b\} : \boldsymbol{\psi}_0|_T \in [P_k(T)]^3, \boldsymbol{\psi}_b|_{\partial T} \in G_k(\partial T), \forall T \in \mathcal{T}_h, \boldsymbol{\psi}_b|_{\Gamma} = 0\},$$

where $G_k(\partial T) := [P_k(\sigma)]^3 \times \mathbf{n}_\sigma$ is the space of polynomials of degree k in the tangent space of ∂T .

For simplicity of notation, for $\sigma \in S_h$ or $\sigma \in M_h$, denote by $\nabla_w \sigma$ the discrete weak gradient $\nabla_{w,k,T} \sigma$ computed by using (3.1) on each element T ; i.e.,

$$(\nabla_w \sigma)|_T = \nabla_{w,k,T}(\sigma|_T), \quad \sigma \in S_h \text{ or } \sigma \in M_h.$$

Analogously, for $\mathbf{q} \in \mathbf{W}_h$, denote by $\nabla_w \times \mathbf{q}$ the discrete weak curl $\nabla_{w,k,T} \times \mathbf{q}$ computed by using (3.2) on each element T ; i.e.,

$$(\nabla_w \times \mathbf{q})|_T = \nabla_{w,k,T} \times (\mathbf{q}|_T), \quad \mathbf{q} \in \mathbf{W}_h.$$

An approximation of the bilinear form $B(\cdot; \cdot)$ is given as follows:

$$(4.1) \quad B_h(\mathbf{u}_h, s_h; \varphi, \boldsymbol{\psi}) := (\mathbf{u}_h, \varepsilon \nabla_w \varphi + \nabla_w \times \boldsymbol{\psi}) + (\boldsymbol{\psi}_0, \varepsilon \nabla_w s_h)$$

for $\mathbf{u}_h \in \mathbf{V}_h$, $s_h \in S_h$, $\varphi \in M_h$, $\boldsymbol{\psi} \in \mathbf{W}_h$.

The following is the PDWG finite element method for the div-curl model system (1.1)-(1.3).

Algorithm 1 (PDWG Algorithm). *For an approximate solution of (1.1)-(1.3), one may compute $\mathbf{u}_h \in \mathbf{V}_h$, together with three auxiliary variables $s_h \in S_h$, $\lambda_h \in M_h$, and $\mathbf{q}_h \in \mathbf{W}_h$ satisfying*

$$(4.2) \quad \begin{cases} s_1(\lambda_h, \mathbf{q}_h; \varphi, \boldsymbol{\psi}) + B_h(\mathbf{u}_h, s_h; \varphi, \boldsymbol{\psi}) = F(\varphi, \boldsymbol{\psi}), & \forall \varphi \in M_h, \boldsymbol{\psi} \in \mathbf{W}_h, \\ -s_2(s_h, r) + B_h(\mathbf{v}, r; \lambda_h, \mathbf{q}_h) = 0, & \forall \mathbf{v} \in \mathbf{V}_h, r \in S_h. \end{cases}$$

Here the stabilizer s_1 is given by

$$(4.3) \quad s_1(\lambda_h, \mathbf{q}_h; \varphi, \boldsymbol{\psi}) = \rho_1 \sum_{T \in \mathcal{T}_h} h_T^{-1} \langle \lambda_0 - \lambda_b, \varphi_0 - \varphi_b \rangle_{\partial T} \\ + \rho_2 \sum_{T \in \mathcal{T}_h} h_T^{-1} \langle \mathbf{q}_0 \times \mathbf{n} - \mathbf{q}_b \times \mathbf{n}, \boldsymbol{\psi}_0 \times \mathbf{n} - \boldsymbol{\psi}_b \times \mathbf{n} \rangle_{\partial T},$$

and s_2 is defined accordingly in the space M_h as follows

$$s_2(s_h; r) = \rho_3 \sum_{T \in \mathcal{T}_h} h_T^{-\gamma} \langle s_0 - s_b, r_0 - r_b \rangle_{\partial T},$$

where $\gamma \geq -1$ and $\rho_i > 0$ are parameters with values at user's discretion.

The PDWG scheme (4.2) further provides an approximation of the space of normal ε -harmonic vector fields $\mathbb{H}_{\varepsilon n, 0}(\Omega)$, as revealed by Theorem 6.2 in that the difference $\boldsymbol{\eta}_h = \mathcal{Q}_h \mathbf{u} - \mathbf{u}_h$ is sufficiently close to a true normal ε -harmonic vector field $\boldsymbol{\eta}$. For this purpose, we introduce the following notation of discrete normal ε -harmonic functions.

Definition 4.1 (discrete normal ε -harmonic functions). A vector field $\boldsymbol{\eta}_h \in \mathbf{V}_h$ is said to be a discrete normal ε -harmonic function if there exists a vector field $\mathbf{u} \in H(\operatorname{div}_\varepsilon; \Omega) \cap H(\operatorname{curl}; \Omega)$ such that

$$(4.4) \quad \boldsymbol{\eta}_h = \mathcal{Q}_h \mathbf{u} - \mathbf{u}_h,$$

where \mathcal{Q}_h is the L^2 projection operator onto the finite element space \mathbf{V}_h and \mathbf{u}_h is the solution of (4.2) for a div-curl system (1.1)-(1.3) with load functions f , \mathbf{g} , and ϕ_1 determined by \mathbf{u} .

In practical computation, a discrete normal ε -harmonic function can be readily obtained from (4.4) by choosing a smooth vector field \mathbf{u} and one solving of the PDWG system (4.2).

5. SOLUTION EXISTENCE AND UNIQUENESS

Introduce two semi-norms as follows:

$$(5.1) \quad \|(\lambda_h, \mathbf{q}_h)\| = \left(s_1(\lambda_h, \mathbf{q}_h; \lambda_h, \mathbf{q}_h) \right)^{\frac{1}{2}}, \quad \lambda_h \in M_h, \mathbf{q}_h \in \mathbf{W}_h,$$

$$(5.2) \quad \|s_h\| = \left(s_2(s_h; s_h) \right)^{\frac{1}{2}}, \quad s_h \in S_h.$$

For simplicity, assume that ε is piecewise constant with respect to the partition \mathcal{T}_h . Note that all the results can be generalized to piecewise smooth ε without any difficulty.

Denote by Q_0 the L^2 projection operator onto $P_k(T)$ and Q_b the L^2 projection operator onto $P_k(\sigma)$ on each face $\sigma \in \partial T$. Denote by Q_h the projection operator onto the weak finite element space S_h or M_h such that

$$(Q_h w)|_T = \{Q_0 w|_T, Q_b w|_{\partial T}\}.$$

Analogously, we use \mathbb{Q}_0 , \mathbb{Q}_b and \mathbb{Q}_h to denote the L^2 projection operators onto $[P_k(T)]^3$, $G_k(\sigma) = [P_k(\sigma)]^3 \times \mathbf{n}_\sigma$, and \mathbf{W}_h , respectively. The L^2 projection operator onto the finite element space \mathbf{V}_h is denoted as \mathcal{Q}_h .

Lemma 5.1. [27] *The L^2 projections Q_h and \mathcal{Q}_h satisfy the commutative property*

$$(5.3) \quad \nabla_w(Q_h w) = \mathcal{Q}_h(\nabla w), \quad \forall w \in H^1(T),$$

$$(5.4) \quad \nabla_w \times (\mathbb{Q}_h \boldsymbol{\psi}) = \mathcal{Q}_h(\nabla \times \boldsymbol{\psi}), \quad \forall \boldsymbol{\psi} \in H(\operatorname{curl}; T).$$

Theorem 5.2. *The kernel of the matrix of the PDWG finite element scheme (4.2) is given by*

$$K_h = \{(\mathbf{v}_h, s_h = 0, \lambda_h = 0, \mathbf{q}_h = 0) : \mathbf{v}_h \in \mathbf{V}_h \cap \mathbb{H}_{\varepsilon n, 0}(\Omega)\}.$$

In other words, the kernel of the matrix of the PDWG scheme (4.2) is isomorphic to the subspace of $\mathbb{H}_{\varepsilon n, 0}(\Omega)$ consisting of harmonic functions that are piecewise polynomial of degree k .

Proof. Let $(\mathbf{u}_h, s_h, \lambda_h, \mathbf{q}_h)$ be a solution of (4.2) with homogeneous data. It follows that

$$(5.5) \quad s_1(\lambda_h, \mathbf{q}_h; \lambda_h, \mathbf{q}_h) = 0, \quad s_2(s_h, s_h) = 0,$$

$$(5.6) \quad (\mathbf{u}_h, \varepsilon \nabla_w \varphi + \nabla_w \times \boldsymbol{\psi}) + (\boldsymbol{\psi}_0, \varepsilon \nabla_w s_h) = 0, \quad \forall \varphi \in M_h, \boldsymbol{\psi} \in \mathbf{W}_h,$$

$$(5.7) \quad (\mathbf{q}_0, \varepsilon \nabla_w r) + (\mathbf{v}, \varepsilon \nabla_w \lambda_h + \nabla_w \times \mathbf{q}_h) = 0, \quad \forall \mathbf{v} \in \mathbf{V}_h, r \in S_h.$$

From (5.5) we have

$$(5.8) \quad \lambda_0 = \lambda_b, \quad \mathbf{q}_0 \times \mathbf{n} = \mathbf{q}_b \times \mathbf{n}, \quad s_0 = s_b, \quad \text{on } \partial T,$$

so that $\lambda_0 \in C(\Omega)$, $s_0 \in C(\Omega)$ and $\mathbf{q}_0 \in H_0(\text{curl}; \Omega)$. Hence,

$$(5.9) \quad \nabla \lambda_0 = \nabla_w \lambda_h, \quad \nabla \times \mathbf{q}_0 = \nabla_w \times \mathbf{q}_h.$$

Next, by letting $r = 0$ and varying \mathbf{v} in (5.7) we have

$$\varepsilon \nabla_w \lambda_h + \nabla_w \times \mathbf{q}_h = 0,$$

which, together with (5.9), implies

$$(5.10) \quad \varepsilon \nabla \lambda_0 + \nabla \times \mathbf{q}_0 = 0.$$

From $\mathbf{q}_0 \in H_0(\text{curl}; \Omega)$, we have

$$\begin{aligned} (\varepsilon \nabla \lambda_0 + \nabla \times \mathbf{q}_0, \nabla \lambda_0) &= (\varepsilon \nabla \lambda_0, \nabla \lambda_0) + (\nabla \times \mathbf{q}_0, \nabla \lambda_0) \\ &= (\varepsilon \nabla \lambda_0, \nabla \lambda_0) + \langle \mathbf{n} \times \mathbf{q}_0, \lambda_0 \rangle \\ &= (\varepsilon \nabla \lambda_0, \nabla \lambda_0). \end{aligned}$$

Thus,

$$(\varepsilon \nabla \lambda_0, \nabla \lambda_0) = 0,$$

which gives $\nabla \lambda_0 = \mathbf{0}$, and hence $\lambda_0 \equiv 0$ as a function with mean value 0. This further leads to $\lambda_b \equiv 0$. Thus, from (5.10) we have

$$\nabla \times \mathbf{q}_0 = 0, \quad \text{in } \Omega.$$

Observe that \mathbf{q}_0 satisfies

$$(\mathbf{q}_0, \varepsilon \nabla_w r) = 0 \quad \forall r \in S_h,$$

which leads to $\mathbf{q}_0 \in H(\text{div}_\varepsilon; \Omega)$ and

$$\nabla \cdot (\varepsilon \mathbf{q}_0) = 0, \quad \langle \mathbf{q}_0 \cdot \mathbf{n}_i, 1 \rangle_{\Gamma_i} = 0,$$

for $i = 1, 2, \dots, L$. This, together with $\nabla \times \mathbf{q}_0 = 0$ and $\mathbf{q}_0 \in H_0(\text{curl}; \Omega)$ shows that $\mathbf{q}_0 \equiv \mathbf{0}$, and hence $\mathbf{q}_b = \mathbf{n} \times (\mathbf{q}_b \times \mathbf{n}) = \mathbf{n} \times \mathbf{0} = \mathbf{0}$.

Next, from the Helmholtz decomposition (A.1), we have

$$\mathbf{u}_h = \varepsilon^{-1} \nabla \times \tilde{\boldsymbol{\psi}} + \nabla \tilde{\phi} + \tilde{\boldsymbol{\eta}},$$

with some $\tilde{\boldsymbol{\eta}} \in \mathbb{H}_{\varepsilon n, 0}(\Omega)$ and $\tilde{\boldsymbol{\psi}} \in H_0(\text{curl}; \Omega)$ satisfying $\nabla \cdot (\varepsilon \tilde{\boldsymbol{\psi}}) = 0$ and $\langle \varepsilon \tilde{\boldsymbol{\psi}} \cdot \mathbf{n}_i, 1 \rangle_{\Gamma_i} = 0$ for $i = 1, \dots, L$. From $s_2(s_h, s_h) = 0$ we have $s_0 = s_b$ on ∂T for each element $T \in \mathcal{T}_h$ so that $s_0 \in H^1(\Omega)$. It follows that $\nabla_w s_h = \nabla s_0$. If $\mathbb{H}_{\varepsilon n, 0}(\Omega)$ has dimension 0, then $\tilde{\boldsymbol{\eta}} = \mathbf{0}$. In

(5.6), by choosing the test function ϕ and ψ to be the L^2 projection of the corresponding function in the Helmholtz decomposition we arrive at

$$\begin{aligned}
 0 &= (\mathbf{u}_h, \varepsilon \nabla_w \mathcal{Q}_h \tilde{\varphi} + \nabla_w \times \mathcal{Q}_h \tilde{\psi}) + (\mathcal{Q}_0 \tilde{\psi}, \varepsilon \nabla_w s_h) \\
 &= (\mathbf{u}_h, \mathcal{Q}_h \varepsilon \nabla \tilde{\varphi} + \mathcal{Q}_h \nabla \times \tilde{\psi}) + (\tilde{\psi}, \varepsilon \nabla s_0) \\
 (5.11) \quad &= (\mathbf{u}_h, \varepsilon \nabla \tilde{\varphi} + \nabla \times \tilde{\psi}) + (\tilde{\psi}, \varepsilon \nabla s_0) \\
 &= (\varepsilon \mathbf{u}_h, \mathbf{u}_h - \tilde{\boldsymbol{\eta}}) + (\tilde{\psi}, \varepsilon \nabla s_0) \\
 &= (\varepsilon (\mathbf{u}_h - \tilde{\boldsymbol{\eta}}), \mathbf{u}_h - \tilde{\boldsymbol{\eta}}),
 \end{aligned}$$

which leads to $\mathbf{u}_h - \tilde{\boldsymbol{\eta}} = 0$; i.e., \mathbf{u}_h is a harmonic function. As a harmonic function and piecewise polynomial of degree k , the first term on the left-hand side of (5.6) becomes to be zero for all test functions $\varphi \in M_h$ and $\psi \in \mathbf{W}_h$. It follows that $\nabla_w s_h = 0$ so that $\nabla s_0 = \nabla_w s_h = 0$ and hence $s_0 \equiv 0$, so is $s_b \equiv 0$. \square

The following is our main result concerning the solution existence and uniqueness of the numerical scheme (4.2).

Theorem 5.3. *The PDWG finite element scheme (4.2) has one and only one solution for all the components except \mathbf{u}_h . The solution \mathbf{u}_h is unique up to a discrete harmonic function $\boldsymbol{\eta}_h \in \mathbb{H}_{\varepsilon n, 0}(\Omega)$ that is a piecewise polynomial of degree k .*

For the PDWG element of lowest order (i.e., $k = 0$), a discrete harmonic function $\boldsymbol{\eta}_h \in \mathbb{H}_{\varepsilon n, 0}(\Omega)$ would be a piecewise constant vector field that is continuous across each interior element interface and has vanishing value on the domain boundary along the normal direction. It follows that one must have $\boldsymbol{\eta}_h \equiv 0$, or equivalently, the PDWG finite element scheme (4.2) has one and only one solution for all the components.

6. ERROR ANALYSIS

For the exact solution $\{\mathbf{u}; s = 0\}$ of the div-curl system, we have from (3.1) and (3.2) that

$$\begin{aligned}
 B_h(\mathcal{Q}_h \mathbf{u}, \mathcal{Q}_h s; \varphi, \psi) &= (\mathcal{Q}_h \mathbf{u}, \varepsilon \nabla_w \varphi + \nabla_w \times \psi) + (\psi_0, \varepsilon \nabla_w \mathcal{Q}_h s) \\
 &= (\mathcal{Q}_h \mathbf{u}, \varepsilon \nabla \varphi_0 + \nabla \times \psi_0) \\
 &\quad + \langle \mathcal{Q}_h \mathbf{u}, \varepsilon \mathbf{n}(\varphi_b - \varphi_0) + (\psi_0 - \psi_b) \times \mathbf{n} \rangle_{\partial \mathcal{T}_h} \\
 &= (\mathbf{u}, \varepsilon \nabla \varphi_0 + \nabla \times \psi_0) \\
 &\quad + \langle \mathcal{Q}_h \mathbf{u}, \varepsilon \mathbf{n}(\varphi_b - \varphi_0) + (\psi_0 - \psi_b) \times \mathbf{n} \rangle_{\partial \mathcal{T}_h} \\
 (6.1) \quad &= -(\nabla \cdot (\varepsilon \mathbf{u}), \varphi_0) + (\nabla \times \mathbf{u}, \psi_0) \\
 &\quad + \langle \mathbf{u}, \varepsilon \mathbf{n}(\varphi_0 - \varphi_b) + (\psi_b - \psi_0) \times \mathbf{n} \rangle_{\partial \mathcal{T}_h} \\
 &\quad + \langle \mathcal{Q}_h \mathbf{u}, \varepsilon \mathbf{n}(\varphi_b - \varphi_0) + (\psi_0 - \psi_b) \times \mathbf{n} \rangle_{\partial \mathcal{T}_h} \\
 &\quad + \langle \phi_1, \varphi_b \rangle_{\partial \Omega} \\
 &= \langle \phi_1, \varphi_b \rangle_{\partial \Omega} - (f, \varphi_0) + (\mathbf{g}, \psi_0) \\
 &\quad + \langle \mathbf{u} - \mathcal{Q}_h \mathbf{u}, \varepsilon \mathbf{n}(\varphi_0 - \varphi_b) + (\psi_b - \psi_0) \times \mathbf{n} \rangle_{\partial \mathcal{T}_h}.
 \end{aligned}$$

Combining the above equation with the fact that $\lambda = 0$, $\mathbf{q} = 0$ we obtain

$$\begin{aligned}
 (6.2) \quad & s_1(\mathcal{Q}_h \lambda - \lambda_h, \mathcal{Q}_h \mathbf{q} - \mathbf{q}_h; \varphi, \psi) + B(\mathcal{Q}_h \mathbf{u} - \mathbf{u}_h, \mathcal{Q}_h s - s_h; \varphi, \psi) \\
 &= \langle \mathbf{u} - \mathcal{Q}_h \mathbf{u}, \varepsilon \mathbf{n}(\varphi_0 - \varphi_b) + (\psi_b - \psi_0) \times \mathbf{n} \rangle_{\partial \mathcal{T}_h}.
 \end{aligned}$$

The second error equation can be easily obtained as follows:

$$(6.3) \quad -s_2(Q_h s - s_h, r) + B(\mathbf{v}, r; Q_h \lambda - \lambda_h, \mathbb{Q}_h \mathbf{q} - \mathbf{q}_h) = 0,$$

where we have used the fact that $s = 0$, $\mathbf{q} = 0$, and $\lambda = 0$.

Denote the error functions by

$$e_{\mathbf{u}} = \mathbb{Q}_h \mathbf{u} - \mathbf{u}_h, \quad e_s = Q_h s - s_h, \quad e_\lambda = Q_h \lambda - \lambda_h, \quad e_{\mathbf{q}} = \mathbb{Q}_h \mathbf{q} - \mathbf{q}_h.$$

Theorem 6.1. *For the numerical solution \mathbf{u}_h , s_h , λ_h , \mathbf{q}_h arising from the PDWG scheme (4.2), the following estimate holds true:*

$$(6.4) \quad \|(e_\lambda, e_{\mathbf{q}})\| + \|e_s\| \lesssim h^{k+\theta} \|\mathbf{u}\|_{k+\theta},$$

provided that $\mathbf{u} \in [H^{k+\theta}(\Omega)]^3$ for $\theta \in (1/2, 1]$.

Proof. From (6.2) and (6.3) we have

$$s_1(e_\lambda, e_{\mathbf{q}}; e_\lambda, e_{\mathbf{q}}) + s_2(e_s, e_s) = \langle \mathbf{u} - \mathbb{Q}_h \mathbf{u}, \varepsilon \mathbf{n} (e_{\lambda,0} - e_{\lambda,b}) + (e_{\mathbf{q},b} - e_{\mathbf{q},0}) \times \mathbf{n} \rangle_{\partial \mathcal{T}_h},$$

which leads to

$$(6.5) \quad \|(e_\lambda, e_{\mathbf{q}})\|^2 + \|e_s\|^2 \lesssim h^{k+\theta} \|\mathbf{u}\|_{k+\theta} \|(e_\lambda, e_{\mathbf{q}})\|,$$

where $\theta \in (1/2, 1]$ and k is the order of polynomials for the finite element space \mathbf{V}_h . This completes the proof of the theorem. \square

To derive an estimate for the error function $e_{\mathbf{u}}$, we use the Helmholtz decomposition (A.1) to obtain a $\tilde{\phi} \in H^1(\Omega)$, $\tilde{\psi} \in H_0(\text{curl}; \Omega)$, and $\tilde{\boldsymbol{\eta}} \in \mathbb{H}_{\varepsilon n, 0}(\Omega)$ such that

$$(6.6) \quad e_{\mathbf{u}} = \varepsilon^{-1} \nabla \times \tilde{\psi} + \nabla \tilde{\phi} + \tilde{\boldsymbol{\eta}}.$$

Assume the following H^α -regularity holds true for some fixed $\alpha \in (1/2, 1]$:

$$(6.7) \quad \|\tilde{\psi}\|_\alpha + \|\tilde{\phi}\|_\alpha \lesssim \|e_{\mathbf{u}} - \tilde{\boldsymbol{\eta}}\|_0.$$

The following is the main convergence result of this paper.

Theorem 6.2. *Let \mathbf{u} be a solution of the div-curl system (1.1)-(1.3). Assume that the Helmholtz decomposition (6.6) has the H^α -regularity estimate (6.7). For a numerical solution \mathbf{u}_h , s_h , λ_h , \mathbf{q}_h arising from (4.2), there exists a harmonic function $\boldsymbol{\eta} \in \mathbb{H}_{\varepsilon n, 0}(\Omega)$ such that the following estimate holds true:*

$$(6.8) \quad \|\varepsilon^{1/2}(\mathbf{u}_h + \boldsymbol{\eta} - \mathbb{Q}_h \mathbf{u})\| \lesssim h^{k+\theta+\alpha-1} \|\mathbf{u}\|_{k+\theta},$$

provided that $\mathbf{u} \in [H^{k+\theta}(\Omega)]^3$ for $\theta \in (1/2, 1]$.

Proof. From the first error equation (6.2), we have

$$(6.9) \quad s_1(e_\lambda, e_{\mathbf{q}}; \varphi, \boldsymbol{\psi}) + B(e_{\mathbf{u}}, e_s; \varphi, \boldsymbol{\psi}) = \langle \mathbf{u} - \mathbb{Q}_h \mathbf{u}, \varepsilon \mathbf{n} (\varphi_0 - \varphi_b) + (\boldsymbol{\psi}_b - \boldsymbol{\psi}_0) \times \mathbf{n} \rangle_{\partial \mathcal{T}_h}.$$

By letting $\varphi = Q_h \tilde{\phi}$ and $\boldsymbol{\psi} = \mathbb{Q}_h \tilde{\boldsymbol{\psi}}$, we obtain from Lemma 5.1

$$(6.10) \quad \begin{aligned} B(e_{\mathbf{u}}, e_s; \varphi, \boldsymbol{\psi}) &= (e_{\mathbf{u}}, \varepsilon \nabla_w Q_h \tilde{\phi} + \nabla_w \times \mathbb{Q}_h \tilde{\boldsymbol{\psi}}) + (\mathbb{Q}_0 \tilde{\boldsymbol{\psi}}, \varepsilon \nabla_w e_s) \\ &= (e_{\mathbf{u}}, \varepsilon \mathbb{Q}_h \nabla_w \tilde{\phi} + \mathbb{Q}_h \nabla_w \times \tilde{\boldsymbol{\psi}}) + (\mathbb{Q}_0 \tilde{\boldsymbol{\psi}}, \varepsilon \nabla_w e_s) \\ &= (e_{\mathbf{u}}, \varepsilon \nabla \tilde{\phi} + \nabla \times \tilde{\boldsymbol{\psi}}) + (\mathbb{Q}_0 \tilde{\boldsymbol{\psi}}, \varepsilon \nabla_w e_s) \\ &= (\varepsilon e_{\mathbf{u}}, e_{\mathbf{u}} - \tilde{\boldsymbol{\eta}}) + (\varepsilon \mathbb{Q}_0 \tilde{\boldsymbol{\psi}}, \nabla_w e_s) \\ &= (\varepsilon (e_{\mathbf{u}} - \tilde{\boldsymbol{\eta}}), e_{\mathbf{u}} - \tilde{\boldsymbol{\eta}}) + (\varepsilon \mathbb{Q}_0 \tilde{\boldsymbol{\psi}}, \nabla_w e_s). \end{aligned}$$

From the definition of the weak gradient we have

$$\begin{aligned}
(\varepsilon \mathbb{Q}_0 \tilde{\boldsymbol{\psi}}, \nabla_w e_s) &= (\varepsilon \mathbb{Q}_0 \tilde{\boldsymbol{\psi}}, \nabla e_{s,0}) + \langle \varepsilon \mathbb{Q}_0 \tilde{\boldsymbol{\psi}} \cdot \mathbf{n}, e_{s,b} - e_{s,0} \rangle_{\partial \mathcal{T}_h} \\
&= (\varepsilon \tilde{\boldsymbol{\psi}}, \nabla e_{s,0}) + \langle \varepsilon \mathbb{Q}_0 \tilde{\boldsymbol{\psi}} \cdot \mathbf{n}, e_{s,b} - e_{s,0} \rangle_{\partial \mathcal{T}_h} \\
&= -(\nabla \cdot (\varepsilon \tilde{\boldsymbol{\psi}}), \nabla e_{s,0}) + \langle \varepsilon \tilde{\boldsymbol{\psi}} \cdot \mathbf{n}, e_{s,0} \rangle_{\partial \mathcal{T}_h} + \langle \varepsilon \mathbb{Q}_0 \tilde{\boldsymbol{\psi}} \cdot \mathbf{n}, e_{s,b} - e_{s,0} \rangle_{\partial \mathcal{T}_h} \\
&= \langle \varepsilon \tilde{\boldsymbol{\psi}} \cdot \mathbf{n}, e_{s,0} - e_{s,b} \rangle_{\partial \mathcal{T}_h} + \langle \varepsilon \mathbb{Q}_0 \tilde{\boldsymbol{\psi}} \cdot \mathbf{n}, e_{s,b} - e_{s,0} \rangle_{\partial \mathcal{T}_h} \\
&= \langle \varepsilon (\tilde{\boldsymbol{\psi}} - \mathbb{Q}_0 \tilde{\boldsymbol{\psi}}) \cdot \mathbf{n}, e_{s,0} - e_{s,b} \rangle_{\partial \mathcal{T}_h}.
\end{aligned}$$

Substituting the above into (6.10) then (6.9) yields

$$\begin{aligned}
\|\varepsilon^{1/2}(e_{\mathbf{u}} - \tilde{\boldsymbol{\eta}})\|^2 &= B(e_{\mathbf{u}}, e_s; \varphi, \boldsymbol{\psi}) - \langle \varepsilon (\tilde{\boldsymbol{\psi}} - \mathbb{Q}_0 \tilde{\boldsymbol{\psi}}) \cdot \mathbf{n}, e_{s,0} - e_{s,b} \rangle_{\partial \mathcal{T}_h} \\
&= \langle \mathbf{u} - \mathcal{Q}_h \mathbf{u}, \varepsilon \mathbf{n}(\varphi_0 - \varphi_b) + (\boldsymbol{\psi}_b - \boldsymbol{\psi}_0) \times \mathbf{n} \rangle_{\partial \mathcal{T}_h} - s_1(e_\lambda, e_{\mathbf{q}}; \varphi, \boldsymbol{\psi}) \\
&\quad - \langle \varepsilon (\tilde{\boldsymbol{\psi}} - \mathbb{Q}_0 \tilde{\boldsymbol{\psi}}) \cdot \mathbf{n}, e_{s,0} - e_{s,b} \rangle_{\partial \mathcal{T}_h},
\end{aligned}$$

which leads to

$$\begin{aligned}
\|\varepsilon^{1/2}(e_{\mathbf{u}} - \tilde{\boldsymbol{\eta}})\|^2 &\lesssim h^\theta \|\mathbf{u} - \mathcal{Q}_h \mathbf{u}\|_\theta \|(\varphi, \boldsymbol{\psi})\| + \|(e_\lambda, e_{\mathbf{q}})\| \|(\varphi, \boldsymbol{\psi})\| \\
&\quad + h^{\alpha+(\gamma-1)/2} \|\tilde{\boldsymbol{\psi}}\|_\alpha \|e_s\|.
\end{aligned}$$

It can be proved that

$$\|(\varphi, \boldsymbol{\psi})\| \lesssim h^{\alpha-1} \|(\tilde{\varphi}, \tilde{\boldsymbol{\psi}})\|_\alpha.$$

It follows that

$$\begin{aligned}
\|\varepsilon^{1/2}(e_{\mathbf{u}} - \tilde{\boldsymbol{\eta}})\|^2 &\lesssim h^\theta \|\mathbf{u} - \mathcal{Q}_h \mathbf{u}\|_\theta h^{\alpha-1} \|(\tilde{\varphi}, \tilde{\boldsymbol{\psi}})\|_\alpha + \|(e_\lambda, e_{\mathbf{q}})\| h^{\alpha-1} \|(\tilde{\varphi}, \tilde{\boldsymbol{\psi}})\|_\alpha \\
&\quad + h^{\alpha+(\gamma-1)/2} \|\tilde{\boldsymbol{\psi}}\|_\alpha \|e_s\|.
\end{aligned}$$

so that

$$\begin{aligned}
\|\varepsilon^{1/2}(e_{\mathbf{u}} - \tilde{\boldsymbol{\eta}})\| &\lesssim h^{\alpha+\theta-1} \|\mathbf{u} - \mathcal{Q}_h \mathbf{u}\|_\theta + h^{\alpha-1} \|(e_\lambda, e_{\mathbf{q}})\| + h^{\alpha+(\gamma-1)/2} \|e_s\| \\
&\leq h^{k+\theta+\alpha-1} \|\mathbf{u}\|_{k+\theta},
\end{aligned}$$

which gives rise to the error estimate (6.8). \square

7. NUMERICAL EXPERIMENTS

In this section, we present some numerical results for the PDWG finite element method proposed and analyzed in previous sections. For simplicity, we choose the lowest order PDWG element; i.e., $k = 0$ so that the solution \mathbf{u} is approximated by discontinuous piecewise constant vector fields. The exact solution \mathbf{u} has various regularities ranging from smooth to corner singular. The computational domain includes convex and non-convex polyhedral regions; some have cavities or multiple toroidal topology. The implementation uses an open-source and publicly available MATLAB package iFEM [8]. The computational domain is first partitioned into cubes, and each cube is further divided into 6 tetrahedra of equi-volume to form a shape-regular finite element partition. On each tetrahedral element T with boundary

$\partial T = \cup_{i=1}^4 F_i$, the local finite element space consists of functions given as follows:

$$(7.1) \quad \mathbf{u}_h|_T \in [P_0(T)]^3,$$

$$(7.2) \quad s_h|_T = \{s_0, s_b\} \in \{P_0(T), \Pi_{i=1}^4 P_0(F_i)\},$$

$$(7.3) \quad \varphi_h|_T = \{\varphi_0, \varphi_b\} \in \{P_0(T), \Pi_{i=1}^4 P_0(F_i)\},$$

$$(7.4) \quad \boldsymbol{\psi}_h|_T = \{\boldsymbol{\psi}_0, \boldsymbol{\psi}_b\} \in \{[P_0(T)]^3, T_0(\partial T)\}.$$

Among the spaces above, $T_0(\partial T)$ is tangential to the boundary and is given by

$$T_0(\partial T) := \{\boldsymbol{\psi} : \boldsymbol{\psi}_{F_i,j} \in [P_0(F_i)]^3 \times \mathbf{n}_{F_i}, j = 1, 2 \text{ and } i = 1, 2, 3, 4\},$$

where \mathbf{n}_{F_i} is the outer unit normal vector to face F_i . The basis functions for the first three spaces are straightforward. For $T_0(\partial T)$, on each face F_i we choose the normalized vectors representing the directional vector of any 2 edges ($j = 1, 2$) among 3 on ∂F_i , such that its weak curl is the co-normal vector of this edge with respect to F_i ($i = 1, 2, 3, 4$),

$$\nabla_w \times \{\mathbf{0}, \boldsymbol{\psi}_{F_i,j}\} = 3\boldsymbol{\psi}_{F_i,j} \times (\nabla \zeta_i),$$

where ζ_i is the barycentric coordinate associated with the vertex opposite to face F_i .

For each test problem, we specify a vector field \mathbf{u} as the true solution, while the right-hand side of the div-curl system (1.1)-(1.3) are computed accordingly. We shall evaluate the following errors for the PDWG finite element solution:

$$(7.5) \quad \|\varepsilon^{1/2} \mathbf{e}_u\| := \|\varepsilon^{1/2} (\mathbf{u} - \mathbf{u}_h)\|,$$

$$(7.6) \quad \|(e_\lambda, \mathbf{e}_q)\| := (s_1(\lambda_h, \mathbf{q}_h; \lambda_h, \mathbf{q}_h))^{1/2},$$

$$(7.7) \quad \|e_s\| := (s_2(s_h; s_h))^{1/2},$$

where the $L^2(\Omega)$ -norm $\|\varepsilon^{1/2} \mathbf{e}_u\|$ is computed by using a higher order Gaussian quadrature on each element.

7.1. Example 1. $\Omega = (0, 1)^3$, $\varepsilon = \text{diag}(3, 2, 1)$, the true solution $\mathbf{u} \in (H^1(\Omega))^3$ is given by

$$\mathbf{u}(x, y, z) = \begin{pmatrix} \sin(\pi x) \cos(\pi y) \\ -\sin(\pi y) \cos(\pi x) \\ 0 \end{pmatrix} + \begin{pmatrix} x \\ y \\ z \end{pmatrix}.$$

The performance of the PDWG finite element solution for this test problem is illustrated in Table 1. It can be seen that \mathbf{e}_u , $(e_\lambda, \mathbf{e}_q)$, and e_s all have optimal rate of convergence for $k = 0$ as shown in Theorem 6.2. The plot of the true solution and the PDWG approximation can be found in Figure 1.

TABLE 1. Errors and corresponding rates of convergence for Example 1.

$1/h$	$\ \varepsilon^{1/2} \mathbf{e}_u\ $	rate	$\ (e_\lambda, \mathbf{e}_q)\ $	rate	$\ e_s\ $	rate
2	1.64e-1	–	2.95e-1	–	3.96e-2	–
4	8.16e-2	1.01	1.68e-1	0.82	1.86e-2	1.09
8	3.93e-2	1.03	8.72e-2	0.88	8.79e-3	1.09
16	1.93e-2	1.03	4.41e-2	0.98	4.48e-3	0.98

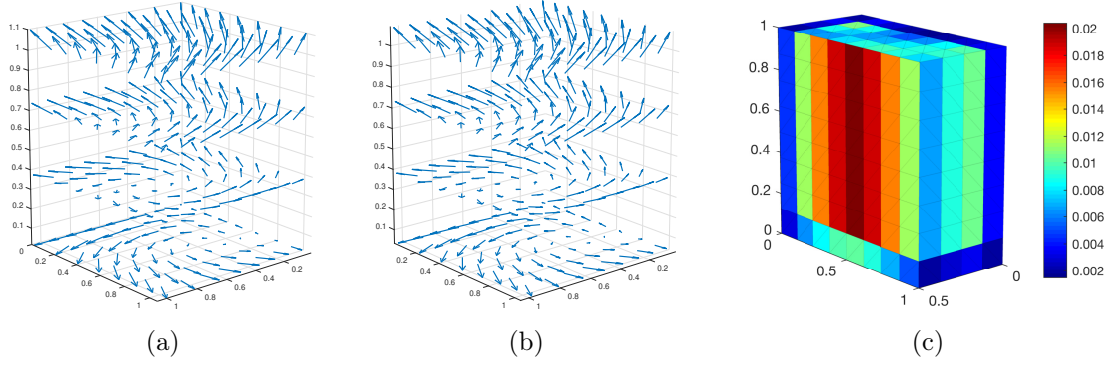


FIGURE 1. The true solution vector field shown in (a) of example 7.1 versus the WG approximation (b). The vector fields are plotted on four $z = c$ planes. The distribution of $\|\varepsilon^{1/2}\mathbf{e}_u\|_T$ locally is plotted in (c) on the cut plane $x = 1/2$ with $h = 1/8$.

7.2. **Example 2.** The second example is adopted from [?] with $\varepsilon = I$ and a singular solution in $(H^{1+\frac{2}{3}-\epsilon}(\Omega))^3$:

$$\mathbf{u}(x, y, z) = \begin{pmatrix} x(1-x) \\ y(1-y) \\ r^{2/3} \sin(2\theta)z(1-z) \end{pmatrix},$$

in which $r = \sqrt{x^2 + y^2}$, and $\theta = \arctan(y/x) + c$ in the cylindrical coordinates. Similar to example 1, the result in Table 2 shows optimal rates of convergence for \mathbf{e}_u , while slightly sub-optimal in the coarsest two levels for $(e_\lambda, \mathbf{e}_q)$, and e_s , respectively. The plot of the true solution and the PDWG approximation can be found in Figure 2.

TABLE 2. Errors and corresponding rates of convergence for Example 2.

$1/h$	$\ \varepsilon^{1/2}\mathbf{e}_u\ $	rate	$\ (e_\lambda, \mathbf{e}_q)\ $	rate	$\ e_s\ $	rate
2	1.13e-1	–	2.07e-1	–	1.74e-2	–
4	5.20e-2	1.12	1.20e-1	0.78	1.05e-2	0.73
8	2.50e-2	1.05	6.27e-2	0.94	5.53e-3	0.93
16	1.23e-2	1.02	3.18e-2	0.98	2.82e-3	0.97

7.3. **Example 3.** This test problem is defined on $\Omega = (-1, 1)^2 \times (0, 1) \setminus [0, 1] \times [-1, 0] \times [0, 1]$ with $\varepsilon = I$ and the singular solution in $(H^{2/3-\epsilon}(\Omega))^3$:

$$\mathbf{u} = \nabla \times \left\langle 0, 0, r^{2/3} \sin\left(\frac{2}{3}\theta\right) \right\rangle.$$

The true solution \mathbf{u} is a solenoidal vector field (see Figure 3). Similar to example 2, $r = \sqrt{x^2 + y^2}$ and $\theta = \arctan(y/x) + c$ are the cylindrical coordinates, where c is chosen such that $\mathbf{u} \in H(\text{div}) \cap H(\text{curl})$. Since $\mathbf{u}(x, y, z)$ has unbounded derivatives as (x, y, z) approaches $\{x = 0, y = 0\} \cap \partial\Omega$, the Gaussian quadrature would yield large error on elements with boundary intersecting z -axis. To overcome this difficulty, we replace the true solution by its

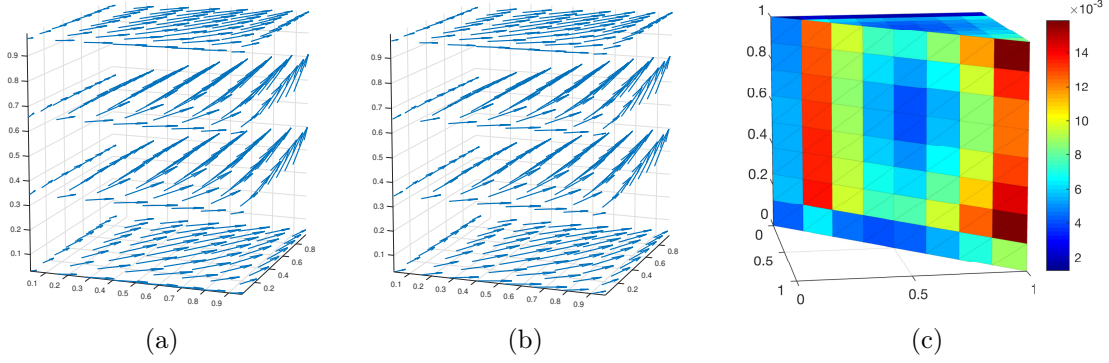


FIGURE 2. The true solution vector field shown in (a) of example 7.2 versus the PDWG approximation (b). The vector fields are plotted on four $z = c$ planes. The distribution of $\|\varepsilon^{1/2}\mathbf{e}_u\|_T$ locally is plotted in (c) on the cut plane $x = y$ with $h = 1/8$.

L^2 -projection in the error computation:

$$\|\varepsilon^{1/2}\mathbf{e}_{Q_h\mathbf{u}}\| := \|\varepsilon^{1/2}(Q_h\mathbf{u} - \mathbf{u}_h)\|.$$

It is observed that $\mathbf{e}_{Q_h\mathbf{u}}$, $(e_\lambda, \mathbf{e}_q)$, and e_s all have maximum possible rate of convergence ($\approx h^{2/3}$) on the finer meshes (see Table 3). The plot of the true solution and the PDWG approximation can be found in Figure 4.

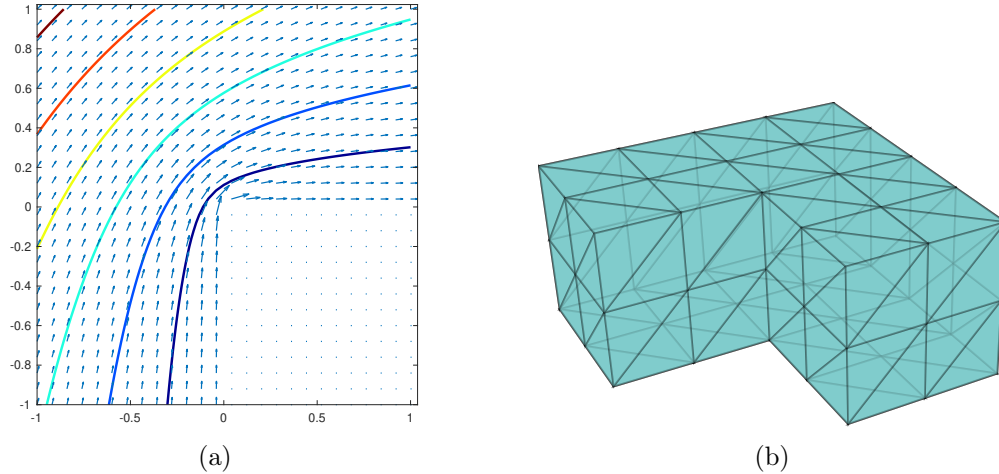


FIGURE 3. The true solution vector field shown in (a) of example 7.3 view from above on $z = 1/4$ plane together with the level set of its z -component. A coarse mesh ($h = 1/2$) used in example 7.3 is illustrated in (b).

7.4. Example 4. This test problem is defined on the domain $\Omega = (-3/2, 1/2)^3 \setminus [-1, 0]^3$ such that the domain boundary $\partial\Omega$ consists of two disjoint connected components $\Gamma_0 = \partial(-3/2, 1/2)^3$ and $\Gamma_1 = \partial(-1, 0)^3$. The true solution is given by

$$\mathbf{u} = \nabla(r^{1/6}), \quad \text{with} \quad r = \sqrt{x^2 + y^2 + z^2}.$$

TABLE 3. Errors and corresponding rates of convergence for Example 3.

$1/h$	$\ \varepsilon^{1/2} \mathbf{e}_{\mathcal{Q}_h \mathbf{u}}\ $	rate	$\ (e_\lambda, \mathbf{e}_q)\ $	rate	$\ e_s\ $	rate
2	5.29e-2	–	3.35e-1	–	4.99e-2	–
4	3.13e-2	0.75	2.19e-1	0.61	3.30e-2	0.60
8	1.91e-2	0.72	1.41e-1	0.63	2.14e-2	0.62
16	1.16e-2	0.72	9.03e-2	0.65	1.37e-2	0.64

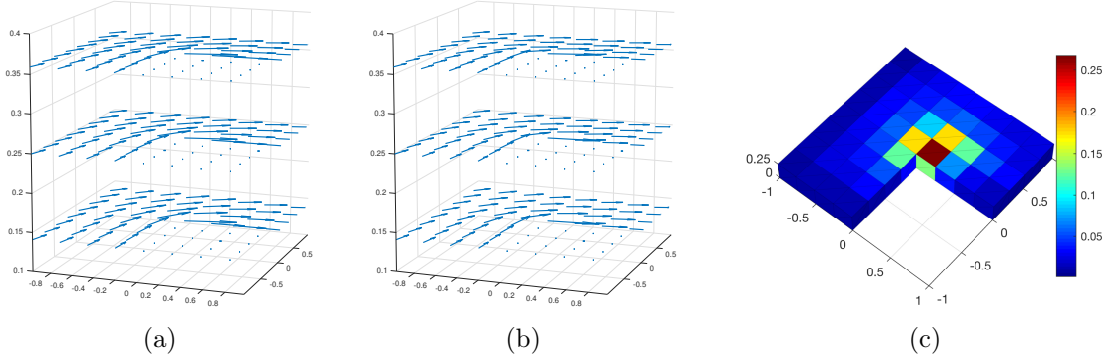


FIGURE 4. The vector field of $\mathcal{Q}_h \mathbf{u}$ is shown in (a) of example 7.3 versus the PDWG approximation (b). The vector fields are plotted on several $z = c$ planes. The distribution of $\|\varepsilon^{1/2} \mathbf{e}_{\mathcal{Q}_h \mathbf{u}}\|_T$ locally is plotted in (c) on the cut plane $z = 1/4$ when $h = 1/8$.

It is straightforward to see that \mathbf{u} is singular near $(0, 0, 0)$ which is one of the nonconvex corners of the cavity (see Figure 5), and $\mathbf{u} \in [H^{2/3-\epsilon}(\Omega)]^3$.

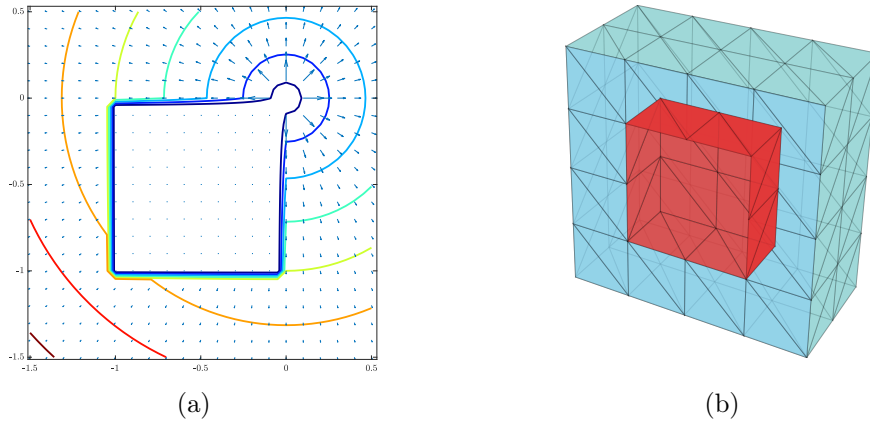


FIGURE 5. (a): plot of the true solution field of example 7.4, view from above on $z = 0$ plane. (b): a coarse mesh ($h = 1/2$) used in example 7.4 cut by the plane $x = 0$, with boundary faces of Γ_1 being highlighted in red.

Table 4 illustrates the convergence of the PDWG method for example 7.4. It can be seen that $\mathbf{e}_{\mathcal{Q}_h \mathbf{u}}$ has the optimal rate of convergence of $O(h^{2/3})$. On the other hand, the

convergence for $(e_\lambda, \mathbf{e}_q)$ and e_s seems to be approximating the optimal rate in this numerical test.

For $s = \{s_0, s_b\}$, when solving the algebraic system, we seek a constant c_1 such that $s_b|_{\Gamma_1} = c_1$ through a simple post-processing by treating $s_b|_{\Gamma_1}$ as the fixed DoFs first. Denote by \mathbf{U} the vector representation of the solution $(\mathbf{u}_h, \lambda_h, s_h, \mathbf{q}_h)$, and $\mathbf{U}_s = c_1 \mathbf{S}$, $\mathbf{S} = (0, \dots, 1, \dots, 1, \dots, 0)$, the indicator vector representing a solution with $s_b = 1$ on Γ_1 while all other DoFs are zero. Let A be the full stiffness matrix including from all nodal bases (including boundary faces), while A^{int} be the stiffness matrix for all the free DoFs: including the interior DoFs for \mathbf{u}_h , s_h , and \mathbf{q}_h , all except 1 fixed DoF for λ_h . Let R be the restriction operator such that $R : \mathbf{U} \mapsto \mathbf{U}^{\text{int}}$, which is the vector representing all the aforementioned free DoFs. First we solve the following algebraic system:

$$A^{\text{int}} \mathbf{U}^{\text{int}} = R \mathbf{F},$$

where \mathbf{F} is the full vector of the right hand side. Then the constant c_1 is sought by solving the following minimization problem:

$$c_1 = \underset{a \in \mathbb{R}}{\operatorname{argmin}} \|A(\mathbf{U}^{\text{int}} + a \mathbf{S}) - \mathbf{F}\|_{\ell^2}.$$

The plot of the projection of the true solution and the PDWG approximation is shown in Figure 6.

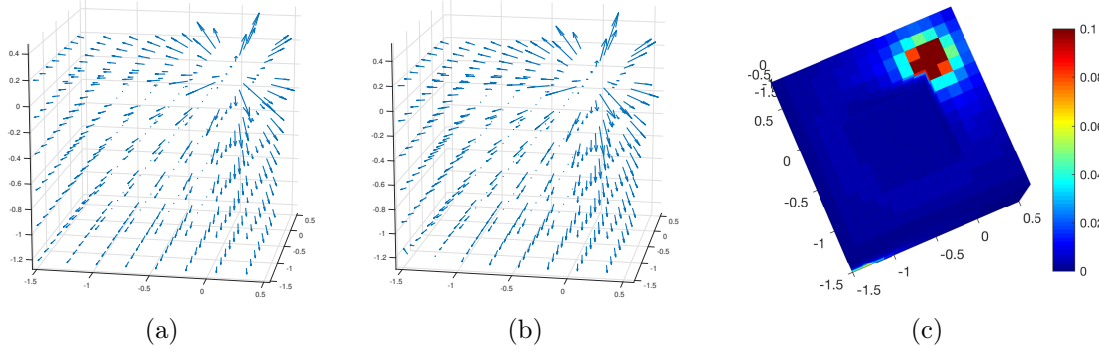


FIGURE 6. Example 7.4: The vector field $\mathcal{Q}_h \mathbf{u}$ is shown in (a) for Example 7.4 versus the PDWG approximation (b). The vector fields are plotted on several $z = c$ planes. The error distribution of $\|\varepsilon^{1/2} \mathbf{e}_{\mathcal{Q}_h \mathbf{u}}\|_T$ is plotted in (c) on the cut plane $z = 0$ with meshsize $h = 1/8$.

TABLE 4. Errors and corresponding rates of convergence for Example 4.

$1/h$	$\ \varepsilon^{1/2} \mathbf{e}_{\mathcal{Q}_h \mathbf{u}}\ $	rate	$\ (e_\lambda, \mathbf{e}_q)\ $	rate	$\ e_s\ $	rate
2	1.90e-1	–	2.51e-1	–	2.04e-2	–
4	1.23e-1	0.63	1.93e-1	0.38	1.69e-2	0.27
8	7.78e-2	0.66	1.35e-1	0.51	1.24e-2	0.44
16	4.91e-2	0.66	9.03e-2	0.58	8.47e-3	0.55

7.5. **Example 5.** In this example we consider singular solutions in the following vector potential form on a toroidal domain with 1 hole: $\Omega = \left((-1, \frac{1}{2})^2 \setminus [-\frac{1}{2}, 0]^2 \times [0, \frac{1}{2}] \right) \times (0, \frac{1}{2})$

$$\mathbf{u} = \nabla \times \langle 0, 0, r^\gamma \sin(\alpha\theta) \rangle,$$

where r and θ are the cylindrical coordinates defined as in Example 7.3. It can be verified that for $\gamma \neq 1$, $\mathbf{u} \in (H^{\gamma-\epsilon}(\Omega))^3$, and for $\gamma < 1$, this vector field is singular near a non-convex corner centered at z -axis (see Figure 7).

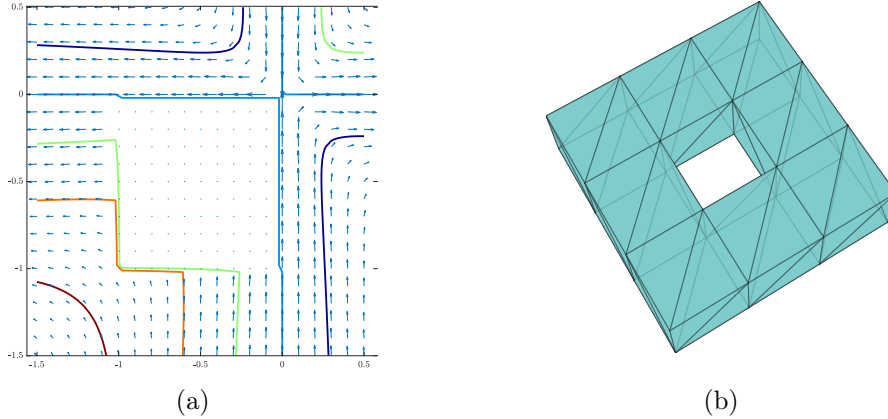


FIGURE 7. Example 7.5: Plot of the singular true solution vector field with $\gamma = 3/4$ and $\alpha = 2$ is shown in (a), view from above on $z = 0$ plane. The level set contours are for the z -component of the vector potential. The coarse mesh ($h = 1/2$) is shown in (b).

Unlike Example 7.3 in which $\gamma = \alpha$ was set on an L-shaped domain, we choose $\alpha = 2$ in this example, so that the resulting vector field is non-harmonic for $\gamma \neq \alpha$, and

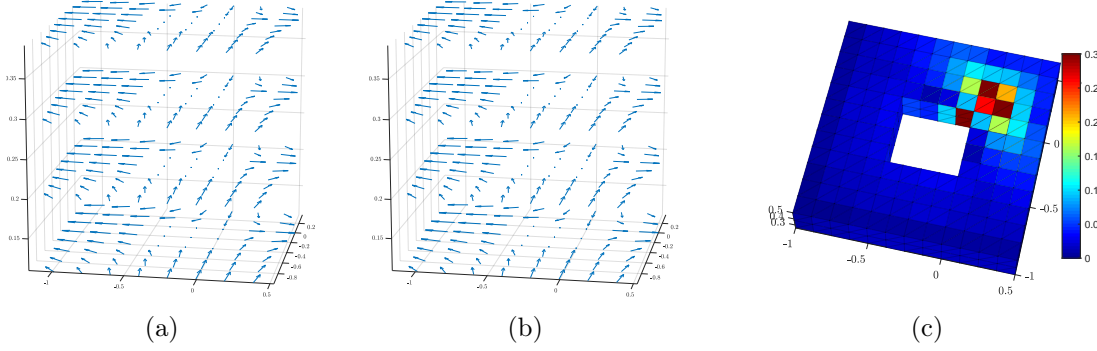
$$\nabla \times \mathbf{u} = \langle 0, 0, -\Delta(r^\gamma \sin(\alpha\theta)) \rangle = \langle 0, 0, (\alpha^2 - \gamma^2)(x^2 + y^2)^{\gamma/2-1} \sin(\alpha\theta) \rangle.$$

Consequently, $\nabla \times \mathbf{u} \notin L^2(\Omega)$ if $\gamma \leq 1$. Nevertheless, due to the unique nature of the PDWG method, we still obtain noteworthy convergence result for the case of $\gamma \leq 1$. In Table 7, we have compiled several cases ranging from smooth to singular and plotted the PDWG approximation vs $\mathcal{Q}_h \mathbf{u}$ in Figure 8.

- *Regular case* $\gamma = 1.25$: $\mathbf{e}_\mathbf{u}$ and e_s show the optimal rates of convergence at $O(h)$, while $\mathbf{e}_{\mathcal{Q}_h \mathbf{u}}$ shows a superconvergence. $(e_\lambda, \mathbf{e}_\mathbf{q})$ only shows a slightly suboptimal rate of convergence during first two refinements, and optimal thereafter.
- *Singular case* $\gamma = 1$: In this case, we have $\mathbf{u} \in H_{loc}^{1-\epsilon}(\Omega)$ and $\mathbf{u} \notin \mathbf{H}(\mathbf{curl})$. $\mathbf{e}_\mathbf{u}$ shows a rate of convergence at $O(h^{0.9})$ asymptotically. Like the smooth case, $\mathbf{e}_{\mathcal{Q}_h \mathbf{u}}$ shows a superconvergence with rates higher than 1. $(e_\lambda, \mathbf{e}_\mathbf{q})$ and e_s show an optimal rate of convergence asymptotically.
- *Singular case* $\gamma = 2/3$: In this case, one has $\mathbf{u} \in H^{2/3-\epsilon}(\Omega)$, and $\mathbf{u} \notin \mathbf{H}(\mathbf{curl})$. Both $\mathbf{e}_\mathbf{u}$ and e_s show optimal rate of convergence at $O(h^{2/3})$. Similarly to previous two cases, $\mathbf{e}_{\mathcal{Q}_h \mathbf{u}}$ exhibits superconvergence with a rate of $O(h^{0.9})$. $(e_\lambda, \mathbf{e}_\mathbf{q})$ shows a convergence with a slightly suboptimal rate of $O(h^{0.6})$.

TABLE 5. Errors and the rates of convergence with different γ for Example 5

	$1/h$	$\ \mathbf{e}_u\ $	rate	$\ \varepsilon^{1/2}\mathbf{e}_{Q_h\mathbf{u}}\ $	rate	$\ (\mathbf{e}_\lambda, \mathbf{e}_q)\ $	rate	$\ e_s\ $	rate
$\gamma = 5/4$ (smooth)	2	3.96e-1	–	1.62e-1	–	9.01e-1	–	8.23e-2	–
	4	2.09e-1	0.92	7.69e-2	1.07	4.94e-1	0.87	5.12e-2	0.68
	8	1.07e-1	0.96	3.23e-2	1.25	2.63e-1	0.91	2.70e-2	0.93
	16	5.44e-2	0.98	1.26e-3	1.35	1.37e-1	0.94	1.32e-2	1.03
$\gamma = 1$ (singular)	2	5.34e-1	–	2.46e-1	–	1.20e0	–	1.42e-1	–
	4	3.06e-1	0.80	1.28e-1	0.94	7.11e-1	0.76	8.95e-2	0.66
	8	1.67e-1	0.87	5.58e-2	1.19	4.04e-1	0.81	4.94e-2	0.86
	16	8.82e-2	0.88	2.55e-2	1.13	2.25e-1	0.85	2.56e-2	0.95
$\gamma = 2/3$ (singular)	2	8.87e-1	–	4.55e-1	–	2.05e0	–	3.41e-1	–
	4	5.87e-1	0.59	2.75e-1	0.73	1.40e0	0.55	2.39e-1	0.51
	8	3.70e-1	0.67	1.39e-1	0.98	9.28e-1	0.60	1.53e-1	0.65
	16	2.34e-1	0.66	7.51e-2	0.89	6.01e-1	0.62	9.51e-2	0.68

FIGURE 8. Example 7.5: The vector field of $Q_h \mathbf{u}$ is shown in (a) versus the PDWG approximation (b) for $\gamma = 2/3$ (singular case). The vector fields are plotted on several $z = c$ planes. The distribution of $\|\varepsilon^{1/2} \mathbf{e}_u\|_T$ locally is plotted in (c) on the cut plane $z = 1/4$ with meshsize $h = 1/8$.

7.6. **Example 6.** In this example we consider a singular solution bearing the same form with that in Example 7.5 on a toroidal domain with 2 holes: $\Omega = [(-1, \frac{3}{2})^2 \setminus \{[-\frac{1}{2}, 0]^2 \times [0, \frac{1}{2}] \cup [\frac{1}{2}, 1] \times [-\frac{1}{2}, 0]\}] \times [0, \frac{1}{2}]$

$$\mathbf{u} = \nabla \times \langle 0, 0, r_1^{\gamma_1} \sin(\alpha\theta_1) + r_2^{\gamma_2} \sin(\alpha\theta_2) \rangle,$$

where (r_i, θ_i) are the cylindrical coordinates centered at a nonconvex corner of the i -th hole, i.e., $r_1 = \sqrt{x^2 + y^2}$, $r_2 = \sqrt{(x-1)^2 + y^2}$, $\theta_1 = \arctan(y/x) + c_1$, and $\theta_2 = \arctan(y/(x-1)) + c_2$. In this example, we choose $\gamma_1 = 1/2$ and $\gamma_2 = 2/3$ such that the vector field is singular near the nonconvex corners of both holes (see Figure 9). In fact, the vector field \mathbf{u} behaves as $H^{1/2-\epsilon}$ -regular in a neighborhood of the edge $\{x = 0, y = 0\}$, and as

$H^{2/3-\epsilon}$ -regular in a neighborhood of the edge $\{x = 1, y = 0\}$. In this example, one has $\mathbf{u} \notin \mathbf{H}(\mathbf{curl})$ as in example 7.5. The convergence results are shown in Table 6. It can be seen that \mathbf{e}_u , $(e_\lambda, \mathbf{e}_q)$, and e_s show optimal rates of convergence at $O(h^{1/2})$. The local error is more prominent near the nonconvex corner of the first hole where \mathbf{u} locally is $H^{1/2-\epsilon}$ -regular (see Figure 10). Similarly to previous two cases, $\mathbf{e}_{\mathcal{Q}_h \mathbf{u}}$ shows superconvergence with a rate approximately at $O(h^{3/4})$.

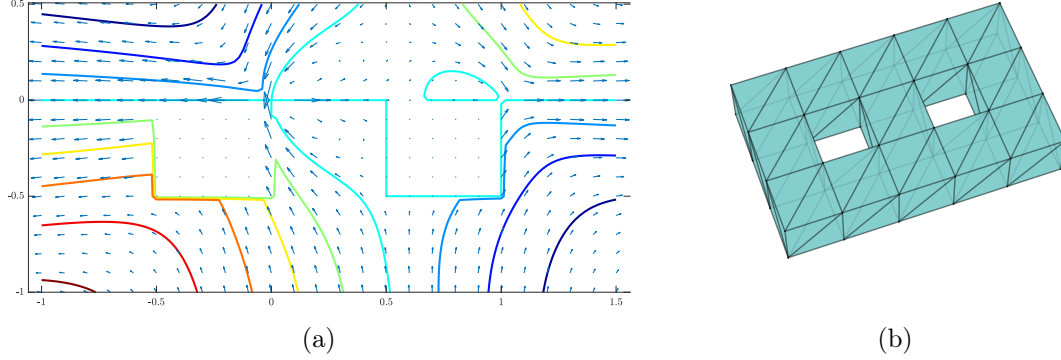


FIGURE 9. Example 7.6: the singular true solution vector field when $\gamma_1 = 1/2$, $\gamma_2 = 2/3$, and $\alpha = 2$ is shown in (a) view from above on $z = 0$ plane. The level set contours are for the z -component of the vector potential used. The coarse mesh ($h = 1/2$) is illustrated in (b).

TABLE 6. Errors and the rates of convergence for Example 6

	$1/h$	$\ \mathbf{e}_u\ $	rate	$\ \varepsilon^{1/2} \mathbf{e}_{\mathcal{Q}_h \mathbf{u}}\ $	rate	$\ (e_\lambda, \mathbf{e}_q)\ $	rate	$\ e_s\ $	rate
$\gamma_1 = 1/2$	2	1.49e0	–	8.37e-1	–	3.39e0	–	6.38e-1	–
	4	1.04e0	0.52	5.18e-1	0.69	2.48e0	0.45	4.74e-1	0.43
$\gamma_2 = 2/3$	8	6.99e-1	0.57	2.84e-1	0.87	1.77e0	0.49	3.27e-1	0.54
	16	4.79e-1	0.55	1.70e-1	0.73	1.24e0	0.51	2.22e-1	0.55

7.7. Example 7. In this example, we report some computational results for a test problem on a toroidal domain with 1 hole. The numerical data does not show a convergence due to the presense of a harmonic vector field, according to Theorem 6.2. The true solution is obtained by combining the ones used in Examples 7.1 and 7.5:

$$\mathbf{u}(x, y, z) = \nabla \times \langle 0, 0, r^\gamma \sin(\alpha\theta) \rangle + \beta \begin{pmatrix} \sin(\pi x) \cos(\pi y) \\ -\sin(\pi y) \cos(\pi x) \\ 0 \end{pmatrix}.$$

In this test, we choose $\alpha = 2$, $\gamma = 2/3$, such that $\mathbf{u} \in \mathbf{H}^{2/3-\epsilon}$, while the extra term with coefficient β is smooth thus not affecting the regularity of the solution. Observe that the extra β term is not divergence free. The optimal rate of convergence should be of order $O(h^{2/3})$ on simply-connected domains unaffected by the β term. As β varies, the numerical results do not demonstrate any convergence for the vector field \mathbf{u} , while optimal order of

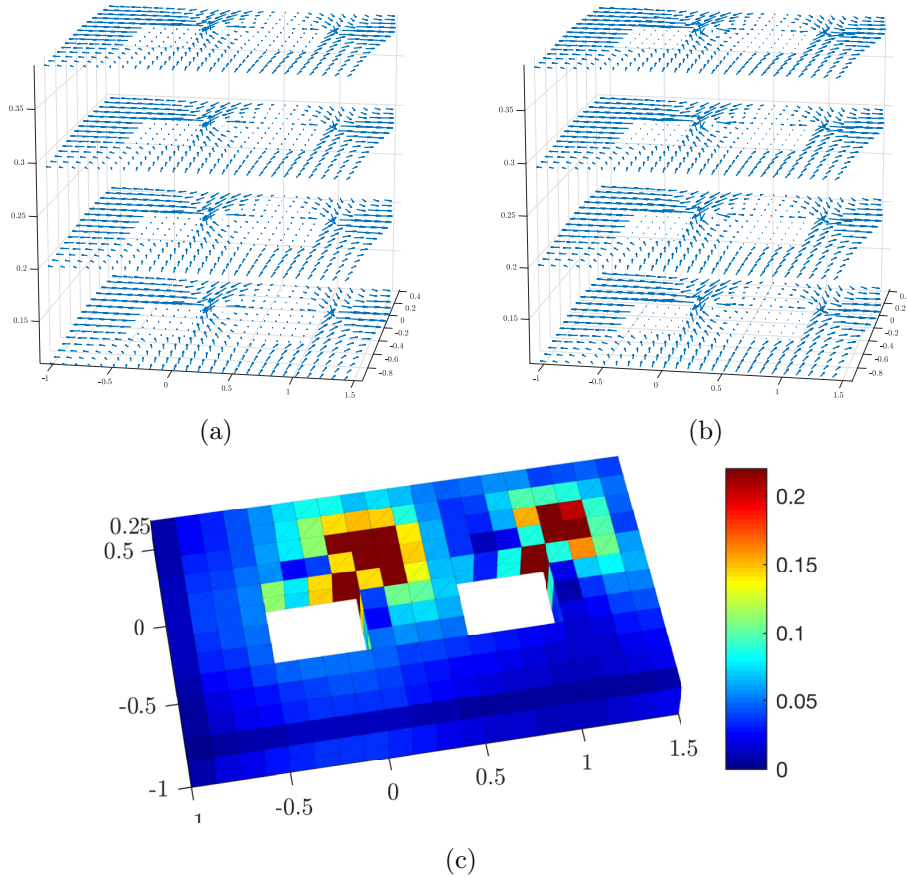


FIGURE 10. Example 7.6: The vector field of $\mathcal{Q}_h \mathbf{u}$ is shown in (a) versus the PDWG approximation (b) for $\gamma_1 = 1/2$ and $\gamma_2 = 2/3$ (singular case). The vector fields are plotted on several $z = c$ planes. The distribution of $\|\varepsilon^{1/2} \mathbf{e}_u\|_T$ locally is plotted in (c) on the cut plane $z = 1/4$ with meshsize $h = 1/8$.

convergence are seen for both $(e_\lambda, \mathbf{e}_q)$ and e_s . The numerical performance is in consistency with our theory as established in Theorem 6.1 for the convergence of $(e_\lambda, \mathbf{e}_q)$ and e_s and Theorem 6.2 for the convergence of the vector field \mathbf{u}_h up to a harmonic field. The vector fields of $\mathcal{Q}_h \mathbf{u}$ and \mathbf{u}_h are plotted in Figure 11 (see (a) and (b)), while their difference $\boldsymbol{\eta}_h = \mathcal{Q}_h \mathbf{u} - \mathbf{u}_h$ is plotted in the same figure as (c). According to Theorem 6.2, the vector field $\boldsymbol{\eta}_h$ is an approximate harmonic field with normal boundary condition.

TABLE 7. Errors and the rates of convergence with different β for Example 7

	$1/h$	$\ \mathbf{e}_u\ $	rate	$\ \varepsilon^{1/2}\mathbf{e}_{Q_h\mathbf{u}}\ $	rate	$\ (e_\lambda, \mathbf{e}_q)\ $	rate	$\ e_s\ $	rate
$\gamma = 2/3$ $\beta = 1$	2	1.26e0	–	8.08e-1	–	2.52e0	–	3.68e-1	–
	4	8.78e-1	0.52	6.35e-1	0.35	1.63e0	0.63	2.54e-1	0.53
	8	6.71e-1	0.39	5.55e-1	0.19	1.03e0	0.66	1.58e-1	0.68
	16	5.82e-1	0.21	5.33e-1	0.06	6.44e-1	0.67	9.72e-2	0.70
	$1/h$	$\ \mathbf{e}_u\ $	rate	$\ \varepsilon^{1/2}\mathbf{e}_{Q_h\mathbf{u}}\ $	rate	$\ (e_\lambda, \mathbf{e}_q)\ $	rate	$\ e_s\ $	rate
$\gamma = 2/3$ $\beta = 5$	2	3.42e0	–	2.75e0	–	5.32e0	–	6.52e-1	–
	4	2.89e0	0.25	2.66e0	0.05	3.16e0	0.75	4.05e-1	0.69
	8	2.71e0	0.09	2.64e0	0.01	1.79e0	0.82	2.21e-1	0.87
	16	2.66e0	0.03	2.64e0	0.00	1.01e0	0.82	1.27e-1	0.80

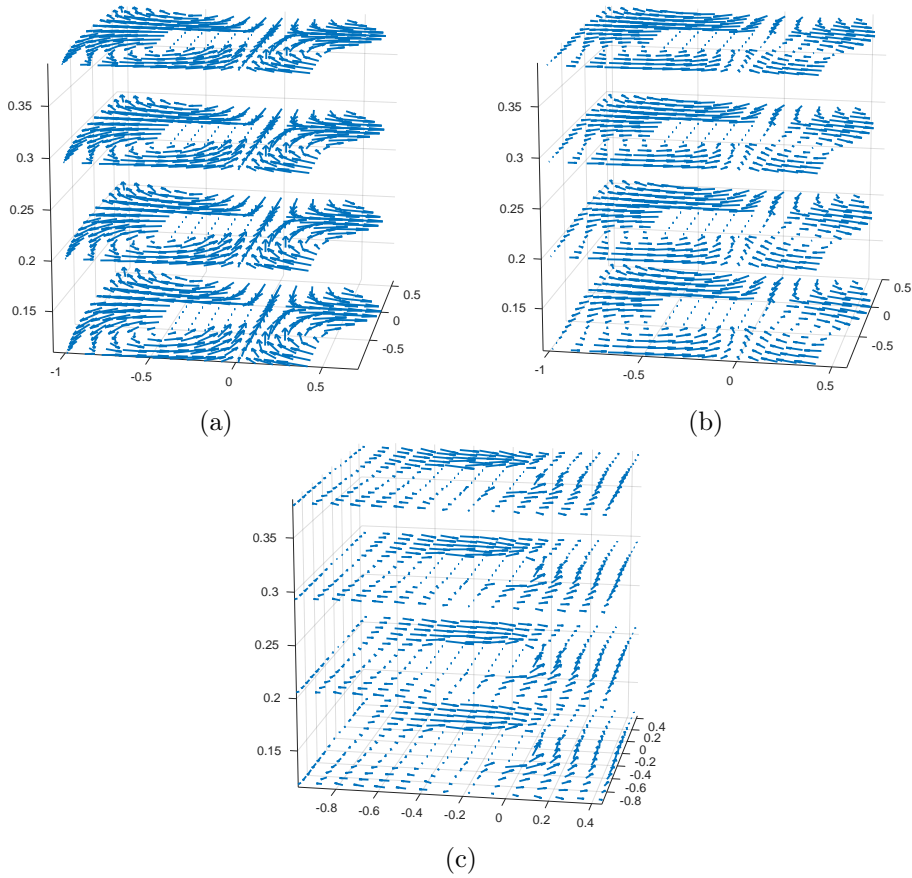


FIGURE 11. Example 7.7: The vector fields of $Q_h \mathbf{u}$ in (a) and that of the PDWG approximation (b) are visually different when \mathbf{u} is not divergence-free on a toroidal domain. The discrete harmonic field $\eta_h = Q_h \mathbf{u} - \mathbf{u}_h$ is plotted in (c). The plots are on several $z = c$ planes.

APPENDIX A. HELMHOLTZ DECOMPOSITION

Theorem A.1. *For any vector-valued function $\mathbf{u} \in [L^2(\Omega)]^3$, there exists a unique $\boldsymbol{\psi} \in H_0(\text{curl}; \Omega)$, $\phi \in H^1(\Omega)/\mathbb{R}$, and $\boldsymbol{\eta} \in \mathbb{H}_{\varepsilon n, 0}(\Omega)$ such that*

$$(A.1) \quad \mathbf{u} = \varepsilon^{-1} \nabla \times \boldsymbol{\psi} + \nabla \phi + \boldsymbol{\eta},$$

$$(A.2) \quad \nabla \cdot (\varepsilon \boldsymbol{\psi}) = 0, \quad \langle \varepsilon \boldsymbol{\psi} \cdot \mathbf{n}_i, 1 \rangle_{\Gamma_i} = 0, \quad i = 1, \dots, L.$$

Moreover, the following estimate holds true

$$(A.3) \quad \|\boldsymbol{\psi}\|_{H(\text{curl}; \Omega)} + \|\nabla \phi\|_0 \lesssim (\varepsilon \mathbf{u}, \mathbf{u})^{\frac{1}{2}}.$$

Proof. The following is a sketch of the proof. Consider the problem of seeking $\boldsymbol{\psi} \in \mathbb{W}_\varepsilon(\Omega)$ such that

$$(A.4) \quad (\varepsilon^{-1} \nabla \times \boldsymbol{\psi}, \nabla \times \boldsymbol{\varphi}) = (\mathbf{u}, \nabla \times \boldsymbol{\varphi}), \quad \forall \boldsymbol{\varphi} \in \mathbb{W}_\varepsilon(\Omega).$$

Denote by

$$a(\boldsymbol{\psi}, \boldsymbol{\varphi}) := (\varepsilon^{-1} \nabla \times \boldsymbol{\psi}, \nabla \times \boldsymbol{\varphi})$$

the bilinear form defined on $\mathbb{W}_\varepsilon(\Omega)$. We claim that $a(\cdot, \cdot)$ is coercive with respect to the $H(\text{curl}; \Omega)$ -norm. To this end, it suffices to derive the following estimate

$$(A.5) \quad \|\mathbf{v}\|_0 \lesssim \|\nabla \times \mathbf{v}\|_0, \quad \mathbf{v} \in \mathbb{W}_\varepsilon(\Omega).$$

In fact, for $\mathbf{v} \in \mathbb{W}_\varepsilon(\Omega)$, from Theorem 3.4 (Chapter 1) of [12], there exists a vector potential function $\boldsymbol{\omega} \in [H^1(\Omega)]^3$ such that

$$(A.6) \quad \varepsilon \mathbf{v} = \nabla \times \boldsymbol{\omega}, \quad \nabla \cdot \boldsymbol{\omega} = 0, \quad \|\boldsymbol{\omega}\|_1 \lesssim (\varepsilon \mathbf{v}, \mathbf{v})^{\frac{1}{2}}.$$

Using the integration by parts and the condition $\mathbf{v} \times \mathbf{n} = 0$ on Γ , we have

$$(\varepsilon \mathbf{v}, \mathbf{v}) = (\nabla \times \boldsymbol{\omega}, \mathbf{v}) = (\boldsymbol{\omega}, \nabla \times \mathbf{v}).$$

It follows from the Cauchy-Schwarz inequality and (A.6) that

$$(\varepsilon \mathbf{v}, \mathbf{v}) \leq \|\boldsymbol{\omega}\|_0 \|\nabla \times \mathbf{v}\|_0 \lesssim (\varepsilon \mathbf{v}, \mathbf{v})^{\frac{1}{2}} \|\nabla \times \mathbf{v}\|_0,$$

which implies (A.5).

Now from the Lax-Milgram Theorem, there exists a unique $\boldsymbol{\psi} \in \mathbb{W}_\varepsilon(\Omega)$ satisfying the equation (A.4) such that

$$\|\boldsymbol{\psi}\|_{H(\text{curl}; \Omega)} \lesssim (\varepsilon \mathbf{u}, \mathbf{u}).$$

It is easy to see that $\mathbb{W}_\varepsilon(\Omega)$ is equivalent to the following quotient space:

$$H_0(\text{curl}; \Omega) / (\nabla H_{0c}^1(\Omega)) = \{\mathbf{v} \in H_0(\text{curl}; \Omega) : (\varepsilon \mathbf{v}, \nabla \phi) = 0, \forall \phi \in H_{0c}^1(\Omega)\}.$$

Thus, by using a Lagrangian multiplier $p \in H_{0c}^1(\Omega)$, the problem (A.4) can be re-formulated as follows: Find $\boldsymbol{\psi} \in H_0(\text{curl}; \Omega)$ and $p \in H_{0c}^1(\Omega)$ such that

$$(A.7) \quad \begin{aligned} (\varepsilon^{-1} \nabla \times \boldsymbol{\psi}, \nabla \times \boldsymbol{\varphi}) + (\varepsilon \nabla p, \boldsymbol{\varphi}) &= (\mathbf{u}, \nabla \times \boldsymbol{\varphi}), \quad \forall \boldsymbol{\varphi} \in H_0(\text{curl}; \Omega), \\ (\boldsymbol{\psi}, \varepsilon \nabla s) &= 0, \quad \forall s \in H_{0c}^1(\Omega). \end{aligned}$$

It follows from the first equation of (A.7) that

$$\nabla \times (\mathbf{u} - \varepsilon^{-1} \nabla \times \boldsymbol{\psi}) - \varepsilon \nabla p = 0.$$

Since $p \in H_{0c}^1(\Omega)$, the two terms on the left-hand side of the above equation are orthogonal in the ε^{-1} -weighted $L^2(\Omega)$ norm. Thus, we have

$$\nabla \times (\mathbf{u} - \varepsilon^{-1} \nabla \times \boldsymbol{\psi}) = 0,$$

which gives

$$\mathbf{u} - \varepsilon^{-1} \nabla \times \boldsymbol{\psi} \in H^0(\text{curl}; \Omega).$$

Thus, there exist unique $\phi \in H^1(\Omega)/\mathbb{R}$ and $\boldsymbol{\eta} \in \mathbb{H}_{\varepsilon n, 0}(\Omega)$ such that

$$\mathbf{u} - \varepsilon^{-1} \nabla \times \boldsymbol{\psi} = \nabla \phi + \boldsymbol{\eta},$$

which completes the proof of the theorem. \square

ACKNOWLEDGEMENT

We would like to express our gratitude to Dr. Long Chen (UCI) for his valuable discussion and suggestions.

REFERENCES

- [1] G. AUCHMUTY AND J.C. ALEXANDER, *L² Well-posedness of planar div-curl systems*, Archive for Rational Mechanics and Analysis, 20 (2001), 160(2), pp. 91-134.
- [2] I. BABUŠKA, *The finite element method with penalty*, Math. Comp., 27 (1973), 221-228.
- [3] R. BENSOW AND M.G. LARSON, *Discontinuous least-squares finite element method for the div-curl problem*, Numer. Math. 101 (2005), pp. 601-617.
- [4] P.B. BOCHEV, K. PETERSON AND C.M. SIEFERT, *Analysis and computation of compatible least-squares methods for div-curl equations*, SIAM J. Numer. Anal., 49 (2011), pp. 159-181.
- [5] J. BRAMBLE AND J.E. PASCIAK, *A new approximation technique for div-curl systems*, Math. Comp. 73 (2004), pp. 1739-1762.
- [6] F. BREZZI, *On the existence, uniqueness, and approximation of saddle point problems arising from Lagrange multipliers*, RAIRO, 8 (1974), 129-151.
- [7] W. CAO AND C. WANG, *New primal-dual weak Galerkin finite element methods for convection-diffusion problems*, arxiv: submit/3011322
- [8] L. CHEN, *iFEM: an innovative finite element methods package in MATLAB*, UC Irvine, 2009, <https://github.com/lyc102/ifem>.
- [9] P.G. CIARLET, *The Finite Element Method for Elliptic Problems*, North-Holland, 1978.
- [10] D.M. COPELAND, J. GOPALAKRISHNAN AND J.E. PASCIAK, *A mixed method for axisymmetric div-curl systems*, Math. Comput., 77 (2008), pp. 1941-1965.
- [11] K.O. FRIEDRICHS, *Differential forms on Riemannian manifolds*, Comm. Pure & Applied Math., vol. 8(1955), 551-590. MR0087763 (19:407a).
- [12] V. GIRAULT AND P-A RAVIART, *Finite Element Methods for Navier-Stokes Equations: Theory and Algorithms*, Springer-Verlag Berlin Heidelberg, 1986.
- [13] D. LI, C. WANG AND J. WANG, *Primal-dual weak Galerkin finite element methods for linear convection equations in non-divergence form*, arXiv: 1910.14073.
- [14] J. LI AND Y. HUANG, *Time-domain finite element methods for Maxwell's equations in metamaterials*, Springer, 2013.
- [15] J. LI, X. YE AND S. ZHANG, *A weak Galerkin least-squares finite element method for div-curl systems*, Journal of Computational Physics, Vol. 363, pp. 79-86. 2018.
- [16] K. LIPNIKOV, G. MANZINI, F. BREZZI AND A. BUFFA, *The mimetic finite difference method for the 3D magnetostatic field problems on polyhedral meshes*, J. Comput. Phys., 230 (2011), pp. 305-328.
- [17] Y. LIU AND J. WANG, *A primal-dual weak Galerkin method for div-curl systems with low-regularity solutions*, arXiv:2003.11795v2.
- [18] R. NICOLAIDES AND X. WU, *Covolume solutions of three-dimensional div-curl equations*, SIAM J. Numer. Anal. 34 (1997) 2195-2203.
- [19] J. SARANEN, *On generalized harmonic fields in domains with anisotropic nonhomogeneous media*, J. Math. Anal. Appl., 88 (1982), pp. 104-115.
- [20] C. WANG, *A new primal-dual weak Galerkin finite element method for ill-posed elliptic Cauchy problems*, Journal of Computational and Applied Mathematics, 2019, available online.
- [21] C. WANG AND J. WANG, *Discretization of div-curl systems by weak Galerkin finite element methods on polyhedral partitions*, J. Sci. Comput. 68 (2016) 1144-1171.

- [22] C. WANG AND J. WANG, *A primal-dual finite element method for first-order transport problems*, Journal of Computational Physics, Vol. 417, 109571, 2020.
- [23] C. WANG AND J. WANG, *A primal-dual weak Galerkin finite element method for second order elliptic equations in non-divergence form*, Math. Comp., 87 (2018) 515-545.
- [24] C. WANG AND J. WANG, *A primal-dual weak Galerkin finite element method for Fokker-Planck type equations*, SIAM J. Numer. Anal., 58(5), 2632-2661. 2020. arXiv:1704.05606.
- [25] C. WANG AND J. WANG, *Primal-dual weak Galerkin finite element methods for elliptic Cauchy problems*, Computers and Mathematics with Applications, vol 79(3), pp. 746-763, 2020.
- [26] C. WANG AND L. ZIKATANOV, *Low regularity primal-dual weak Galerkin finite element methods for convection-diffusion equations*, arXiv:1901.06743.
- [27] J. WANG AND X. YE, *A weak Galerkin mixed finite element method for second-order elliptic problems*, Math. Comp., vol. 83, pp. 2101-2126, 2014.

DEPARTMENT OF MATHEMATICS AND STATISTICS, WASHINGTON UNIVERSITY IN ST. LOUIS, ST. LOUIS, MO 63130

Email address: `s.cao@wustl.edu`

DEPARTMENT OF MATHEMATICS & STATISTICS, TEXAS TECH UNIVERSITY, LUBBOCK, TX 79409, USA

Email address: `chunmei.wang@ttu.edu`

DIVISION OF MATHEMATICAL SCIENCES, NATIONAL SCIENCE FOUNDATION, ALEXANDRIA, VA 22314

Email address: `jwang@nsf.gov`